

Review

Multifunctional Catalysts for Cascade Reactions in Biomass Processing

Lyudmila M. Bronstein ^{1,2,*}  and Valentina G. Matveeva ^{2,3,*} ¹ Department of Chemistry, Indiana University, 800 E. Kirkwood Av., Bloomington, IN 47405, USA² Department of Biotechnology, Chemistry and Standardization, Tver State Technical University, 22 A. Nikitina St., 170026 Tver, Russia³ Regional Technological Centre, Tver State University, Zhelyabova Str., 33, 170100 Tver, Russia

* Correspondence: lybronst@iu.edu (L.M.B.); matveeva@science.tver.ru (V.G.M.)

Abstract: Multifunctional catalysts have received considerable attention in the cascade reactions of biomass processing. A cascade (or tandem) reaction is realized when multiple reaction steps that require different catalysts are performed in a one-step process. These reactions require bi- or multifunctional catalysts or catalyst mixtures to serve successfully at each reaction step. In this review article, we discuss the major factors of the catalyst design influencing the structure–property relationships, which could differ depending on the catalyst type. The major factors include the amounts and strengths of acidic and basic sites, interactions between those and metal sites, synergetic effects, nanoparticle sizes and morphology, nanostructures, porosity, etc. The catalysts described in this review are based on zeolites, mesoporous solids, MOFs, and enzymes. The importance of continuous cascade processes is also examined.

Keywords: multifunctional; cascade reactions; catalysis; acid sites; metal sites; nanoparticles; biomass



Citation: Bronstein, L.M.; Matveeva, V.G. Multifunctional Catalysts for Cascade Reactions in Biomass Processing. *Nanomaterials* **2024**, *14*, 1937. <https://doi.org/10.3390/nano14231937>

Academic Editors: Ioannis Yentekakis, Dimitrios Gournis, Paraskevi Panagiotopoulou and Haralambos Stamatis

Received: 16 November 2024

Revised: 27 November 2024

Accepted: 30 November 2024

Published: 2 December 2024



Copyright: © 2024 by the authors. Licensee MDPI, Basel, Switzerland. This article is an open access article distributed under the terms and conditions of the Creative Commons Attribution (CC BY) license (<https://creativecommons.org/licenses/by/4.0/>).

1. Introduction

With the progress of biomass processing, various types of biomass became promising eco-friendly raw materials capable of replacing non-renewable fossil resources. Normally, biomass processing requires multiple reactions to obtain value-added chemicals or biofuels even if the raw material is a derivative of biomass. To make such processing economically and environmentally feasible, cascade (tandem) reactions were proposed when each catalytic step is carried out in a one-pot reaction. Such reactions require bi- or multifunctional catalysts combining various active sites on the same supports or on the mixture of supports. The major goal of the development of multifunctional catalysts for cascade reactions is the control of selectivity to prevent high energy and labor costs due to separation and purification along with achieving high catalytic activity. This requires catalysts with the well-defined structure of active sites along with a certain porosity, stability, etc. [1–10]. The major reactions of biomass processing include isomerization on Lewis acid sites (LAS) [11–14], esterification on Brønsted acid sites (BAS) [15–19], hydrolysis on both LAS and BAS [20,21], hydration/dehydration on BAS [13,14,17,22,23], hydrodeoxygenation on metal sites and LAS [3,10,24,25], oxidation on metal sites as well as LAS and BAS [11,26–28], hydrogenolysis on LAS, BAS, and metal sites [29,30], and hydrogenation on metal sites and LAS [1,31–33]. It is noteworthy that our review article is focused on the development of multifunctional catalysts and the relationship of the catalyst structure and its catalytic performance in the cascade reactions. The detailed analysis of cascade reactions is beyond the scope of this review, unless it provides an important insight into the key catalyst features.

It is noteworthy that although several research articles on the subject of this review were published before 2014, the explosive development of the field occurred in the last 10 years. That is why, in this review article, we limit our assessment to the last decade by analyzing all trends and findings. In the subsequent sections, we will examine multifunctional catalysts

based on (i) zeolites, (ii) mesoporous solids, (iii) MOFs, and (iv) enzymes. In each section, we will focus on the roles of acid-base and metal sites and their interactions resulting in synergy, site separation, nanoparticle characteristics, porosity, etc. Such a review organization allows us to identify the key factors influencing the cascade reaction of biomass processing.

2. Zeolite-Based Catalysts for Biomass Processing

Zeolites are widely used as catalysts or catalytic supports for biomass processing to biofuels and value-added chemicals [34,35]. Unlike oil raw materials, biomass sources mainly contain cellulose and lignin, whose catalytic transformations are even more challenging. The development of zeolite-based multifunctional nanostructured catalysts and the understanding of their complex structure–property relationships are necessary for the successful cascade catalytic reactions of biomass processing [36].

Due to well-developed porosity zeolites are suitable supports for the stabilization of noble and earth abundant metal and metal oxide nanoparticles (NPs) [37–43]. A combination of the acidic properties of zeolites and metal redox properties leads to the development of universal catalysts with enhanced activity and selectivity. Metal NPs catalyze processes in which hydrogen is involved, including hydrogen activation, hydrogenation, and hydrogen transfer, while acidic sites catalyze hydrolysis, dehydration, ring opening, etc. In this section, we discuss several aspects of the structure of zeolites-based catalysts and their influence on catalysis. The analysis of the review articles published to date shows that zeolites-based catalysts demonstrate an outstanding potential for future industrial applications in biomass processing due their unique BAS/LAS ratios and multifunctional active sites [36,37,44–46].

2.1. Zeolite Types

Zeolite is a natural aluminosilicate with well-ordered pores and a crystal structure [47,48]. Synthetic zeolites, also called molecular sieves, were widely employed for years as absorbents, catalysts, supports for composite materials, etc. [36,44]. Zeolite structures contain different sized rings that determine porosity. In addition to well-defined pore systems with different pore sizes, zeolites possess BAS and LAS, allowing one to obtain various products in acid–base catalytic reactions. They also possess high thermal and chemical stability, making them good candidates as supports for multifunctional catalysts in biomass processing [35,36,44,45].

Three main types of zeolites include MFI (ZSM-5 and HZSM-5) with 10-membered rings, FAU formed by 12-membered ring channels, and BEA (β) also containing 12-membered ring channels of different sizes. MFI zeolites are characterized by two interconnected channel frameworks including pentasil rings with medium pore sizes [49,50]. FAU contain larger pores [51]. The BEA pores are smaller than those of FAU, but larger than the pores of MFI [52]. The pore size determines the diffusion of reacting molecules or filtering out of intermediates to control the reaction outcome. Depending on the Si/Al ratio (aluminum provides negative charges and acidity), the ratio of BAS/LAS can be varied, thus controlling the catalytic properties [53]. Besides classical zeolites discussed above, new variations were developed, such as mesoporous [54–57] and hierarchical zeolites [58–61]. It is worth noting that zeolites can be also alkaline when they undergo an ion exchange with alkaline cations or when they contain inclusions of alkaline metals [62,63].

2.2. The Si/Al Molar Ratio in Zeolites

The variation of the BAS/LAS ratio in zeolites can be achieved by varying the Si/Al ratio [1]. The initial Si/Al ratio is created during the formation of the aluminosilicate framework, which can be influenced at the stage of gel formation [64–66] or in post-synthetic procedures [67].

Desilication, i.e., a removal of some Si species, leads to higher acidity due to BAS (with a counterion). The strength of BAS is higher if they are isolated from each other. On the other hand, using dealumination (removal of Al) can decrease the zeolite acidity. For example, Li et al. reported the catalysts based on dealuminated BEA zeolites, which were

efficient in a cascade reaction of glucose to 5-(ethoxymethyl)furfural (EMF) [68]. It is worth noting that the Si/Al ratio in zeolites can also influence the hydrophilicity/hydrophobicity balance and stability in catalytic processes [15,69,70].

The most impressive influence of the Si/Al ratio was demonstrated in ref. [1] for Pd NPs deposited on H-ZSM-5 and employed in the transformation of biobased furfural (FAL) to cyclopentanone (CPO). Here, the tested Si/Al ratios were 25, 60, 130, and 200. It was demonstrated that the increase in the Si/Al ratio leads to the decrease in the amount and strength of acid sites (both BAS and LAS), resulting in the best catalytic performance (98% selectivity to CPO). A similar effect was observed for Ru-BEA catalysts [71]. With the increase of the Si/Al ratio from 20 to 60, the 2-methylpiperidine (MP) yield (one of the target products of the triacetic acid lactone transformation) increased to 59.8%. The further increase of the Si/Al ratio to 360 led to the decrease of the MP yield.

It would be remiss on our part to ignore that in these complex multifunctional catalysts a single factor (for example, the Si/Al ratio discussed in this section) never determines the reaction result, but it can be a key feature for a particular kind of catalysts and/or reactions.

2.3. Doping of Zeolite Framework

One of the important strategies to modify properties of zeolite-based catalysts and to create multiple active sites is doping with various species. In refs. [45,72] the authors emphasized that multifunctional heteroatomic zeolites with BAS and LAS are necessary in cascade catalytic reactions for stable processes required in industry. In the previous section, we discussed that partial dealumination leads to bifunctional zeolites containing BAS and LAS in a different proportion than in initial zeolites. This could be also achieved by an incorporation of some other ions in the zeolite structure, replacing Al (Figure 1). Dijkmans et. al. synthesized the bifunctional zeolite, Sn-Al-BEA, containing BAS from Al and LAS from Sn [72]. Such Sn-BEA catalysts were efficient in carbon–carbon coupling, carbohydrate isomerization, oxidation reactions, and hydride shift [11]. Sn-BEA showed activity and stability in the Oppenauer oxidation (OPO), Baeyer–Villiger oxidation (BV), and the Meerwein–Ponndorf–Verley (MPV) reaction. Moreover, the cascade reaction including both OPO and BV and carried out by a one-pot method showed an excellent pathway for transforming substituted cyclohexanols obtained from lignin to caprolactone—a precursor for the polyester synthesis [26].

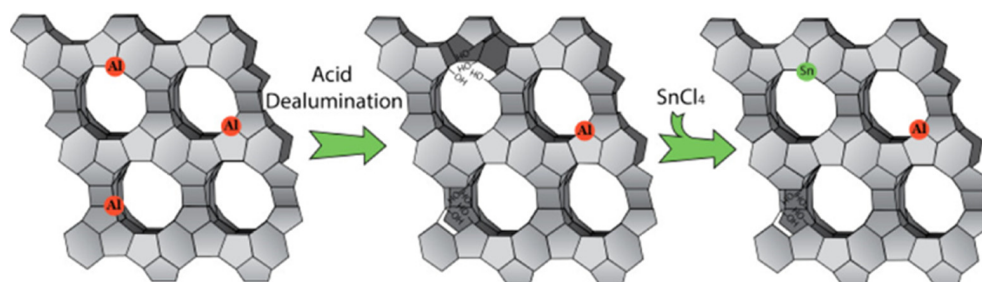


Figure 1. Schematic representation of the synthesis of the materials. Reproduced with permission from [72] the American Chemical Society, 2015.

Analogous Sn-containing BEA were obtained by dealumination with nitric acid and isomorphic replacement of Al with Sn [73]. The proportion of BAS and LAS in Sn-BEA was controlled by the degree of dealumination, which was achieved by varying the concentration and time of the nitric acid treatment. The BAS/LAS ratio, in turn, significantly influenced the selectivity of the cascade reaction of glucose to 5-hydroxymethylfurfural (HMF). The above findings allowed one to formulate optimal acidic properties of the catalysts for the HMF synthesis.

Li et al. reported a new catalyst, CeSn-BEA, doped with Sn and Ce species and containing isolated dual LAS (cations Ce and Sn), which were encapsulated in the matrix of BEA [74]. This work emphasized that dual metal cation sites allow for advantages in

the local environment for biomass processing including C-C coupling with subsequent self-deoxygenation. It was demonstrated that Ce species in BEA (without hydroxyls) are selective in fabrication of isobutene from acetone oligomers when Sn species are present. The authors proposed that coupled dual LAS from Ce and Sn and their local environment stabilizing intermediates are most likely responsible for the stable and selective formation of isobutylene from acetone.

A significant impact of fluorine (via the NH_4F treatment) on bifunctional Pd/HZSM-5 catalysts was described by Jiang et al. [75]. Fluorine substitutes the OH group at the Al site with the formation of the F-Al bond, altering the acid sites, increasing a hydrophobic character of zeolite, and changing the surface structure of the catalyst upon variation of the fluorine amount. The authors demonstrated that the fluorine doping enhanced the catalytic performance in the selective hydrodeoxygenation (HDO) of ketones obtained from biomass. Zhang et al. used a fluorine treatment (via impregnation) of MFI-based composite with Ru NPs to fabricate a catalyst for hydrogenation of levulinic acid (LA) and glucose [76]. An unusual step here is the use of the fluorine compound as seed for the ZSM-5 formation.

A conversion of 2,5-dimethylfuran (DMF) from biomass and ethylene to *p*-xylene (PX) was carried out with HZSM-5, whose BAS/LAS ratio was controlled using ammonium fluoride [77]. The high catalytic activity of this catalyst was explained by hierarchical porosity and specific acidic properties, determined by simultaneous dealumination and desilication during the NH_4F treatment. Hierarchical porosity facilitates reagent diffusion, while appropriate acidity with the optimal ratio of BAS/LAS (1.17) diminishes the DMF hydrolysis (side reaction).

2.4. Incorporation of Metal NPs

As was discussed above, a conversion of biomass to chemicals and fuels often occurs in multiple reactions, each requiring a different active site. For many reactions, a dual action of metal and acid sites is required [46]. The catalysts containing metal NPs and based on zeolites could be finely tuned by a combination of various active sites in order to carry out a multistep reaction in a single pot [36]. Noble metal NPs placed in zeolites (Pd [1], Pt [46], Ru [29,71,78,79]) display high activity and selectivity, while earth-abundant metal or metal alloy NPs allow for cheaper and yet efficient alternatives (Co [24], Ni [80], Ni-Pd [81]). The advantages of the redox properties of metal NPs along with the acidic properties of zeolites allow for the development of catalysts with enhanced activity and selectivity.

The influence of the metal NP size is often crucial in such catalysts, because it controls the number of active sites, associated with the electronic structure and geometry of nanostructured metals [82]. The metal NP size changes the concentration of defects on the NP surface, thus influencing the reagent adsorption, bond cleavage, and bond formation. For example, the incorporation of Cu in Cu-BEA developed for the oxidative cleavage of 1-phenyl-1,2-ethanediol (model reaction of biomass processing) changes the BAS and LAS properties, leading to the target product [83]. In the majority of cases, small NPs provide higher activity due to the increase in the number of active sites and defects [46,84].

In addition to the metal NP size, the NP structure is an important parameter determining catalytic properties. The HZSM-5 based catalysts with different metal NPs were tested in a cascade reaction consisting of dehydroaromatization of terpene limonene and HDO of stearic acid [81]. This cascade reaction first goes through the conversion of terpene to *p*-cymene with simultaneous H_2 formation (Figure 2). After that, one-pot HDO of stearic acid leads to long-chain alkanes (C_{17} and C_{18}). The analysis of various catalysts showed that bimetallic Pd-Ni/HZSM-5 is the best, while monometallic Ni or Pd catalysts showed a poor performance, i.e., a low conversion of stearic acid.

The authors determined that limonene dehydroaromatization is activated by Pd active sites, while stearic acid HDO is catalyzed by Ni. It is noteworthy that HZSM-5 acid sites, which could be altered by changing the Si/Al ratios, impact the Pd-Ni catalytic properties. Also, an appropriate porosity of zeolite inhibits limonene condensation (a side reaction). An additional factor here is an enhanced hydrogen transfer between two metals on the HZSM-5

surface, which improves stearic acid HDO. Thus, both steps of this catalytic reaction are served by the bimetallic zeolite-based catalyst.

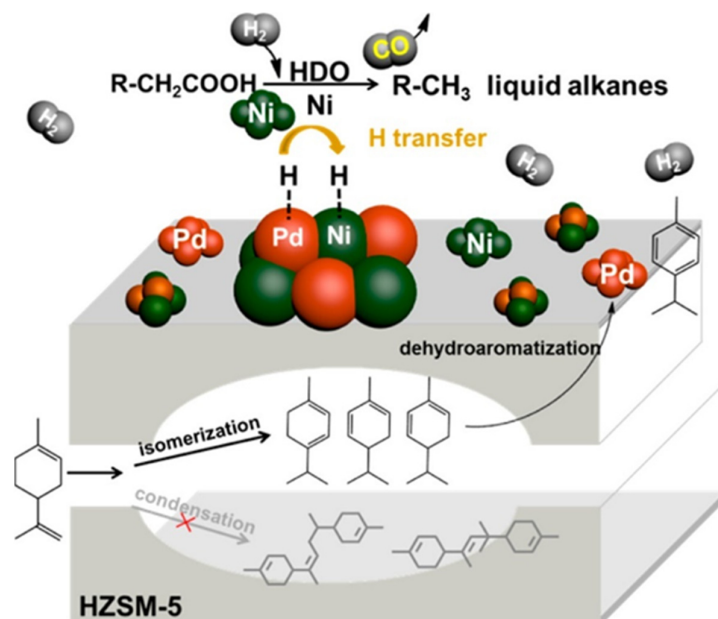


Figure 2. Brief description of individual steps for stearic acid and limonene coactivation using the bimetallic Pd-Ni/HZSM-5 catalyst. Reproduced with permission from [81] the American Chemical Society, 2016.

The other bimetallic catalyst, Co/Sn-BEA, containing metal LAS, was utilized for the selective HDO of HMF to DMF. [24]. Figure 3 depicts the catalyst synthesis.

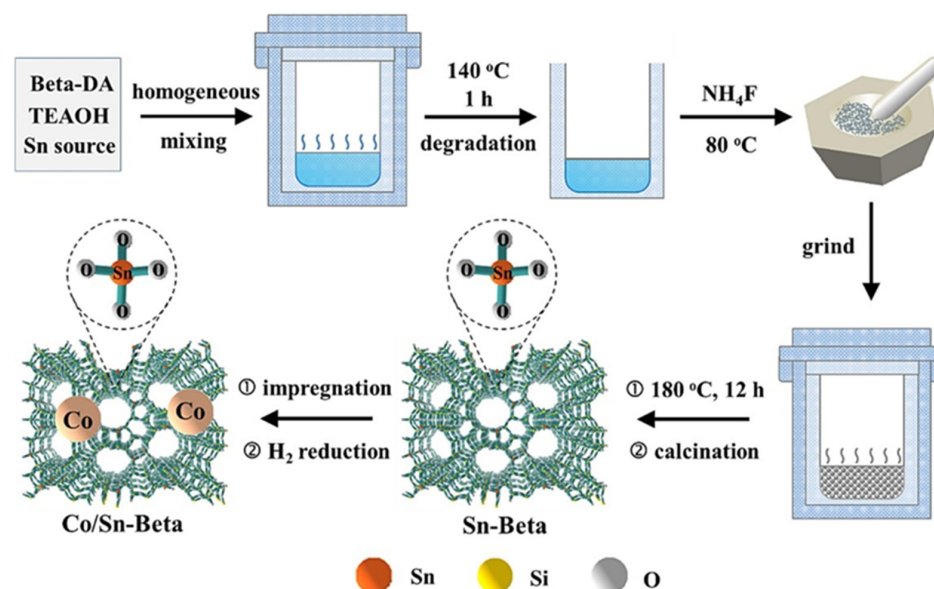


Figure 3. Schematic representation of the preparation procedure for Co/Sn-Beta catalyst. Reproduced with permission from [24] Elsevier, 2024.

In this catalyst, Sn-BEA nanocrystals (30–100 nm in size with a high Sn content) include Co NPs (3–10 nm in diameter) in the zeolite framework, containing many LAS. The analysis of the structure-property relationship showed that Co and Sn concentrations in Co/Sn-BEA are strongly associated with catalytic properties. The role of Co NPs is mostly to control the HMF conversion, while isolated Sn species mainly influence the selectivity to the target

product. Thus, smart control over Co and Sn contents in the catalyst may allow one to efficiently regulate the HMF conversion and DMF selectivity.

Karanwal et al. reported a one-pot reaction of LA to 1,4-pentanediol (1,4-PDO) using Cu-Ni alloy NPs modified by Zn and deposited on H-ZSM-5 (Cu-Ni-Zn/H-ZSM-5) [85]. This catalyst allowed for the 93.4% yield of PDO in optimal conditions. The addition of Zn limited the Cu-Ni NP size to 4–8 nm, making these NPs easier to reduce during hydrogenation than the initial Cu-Ni alloy NPs. A large number of LAS in Cu-Ni-Zn/H-ZSM-5 facilitated the LA adsorption, while the conversion to GVL occurred on BAS of H-ZSM-5. The hydrogenation of LA took place on the Cu-Ni alloy sites. Further ring opening and hydrogenation resulted in PDO, facilitated by H₂ spillover on the Zn-doped Cu-Ni alloy NPs (Figure 4).

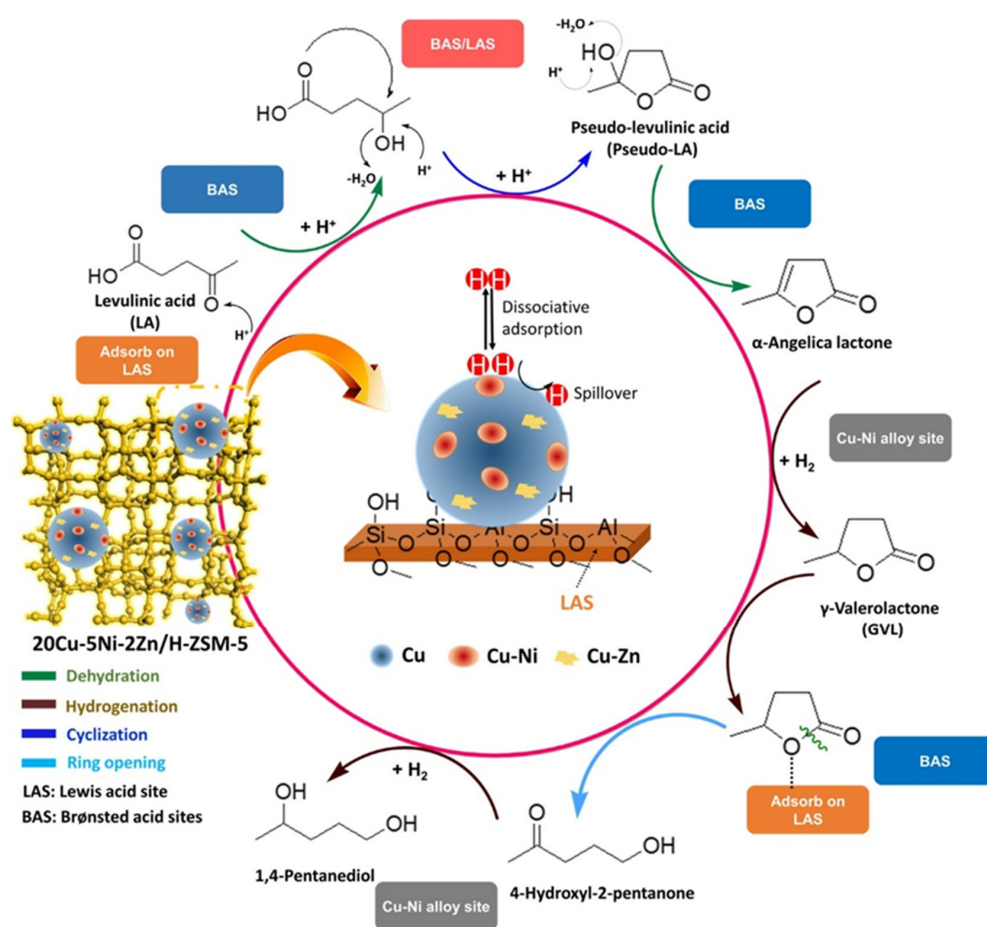


Figure 4. Plausible reaction pathway for the direct conversion of LA to 1,4-PDO over the trimetallic catalyst. Reproduced with permission from [85] the American Chemical Society, 2021.

2.5. Influence of Metal Oxides or Functional Carbons

The incorporation of metal oxides in addition to zeolites could provide additional acid sites which, in conjunction with metal species, enhance multifunctionality of the catalysts. Li et al. developed the Ru-WO_x/HZSM-5 catalyst for cellulose conversion to ethanol [20]. Figure 5 shows the steps of this cascade reaction. Small WO_x NPs allow numerous active sites for selective breakage of the C-C bond in glucose, leading to a transformation to C₂ or C₄ intermediates. Along with WO_x, the formation of small Ru₃W₁₇ alloy NPs (structure is confirmed by X-ray diffraction) provides hydrogenation sites for the successful transformation of glycolaldehyde to ethylene glycol (EG) and EG to ethanol. HZSM-5 acid sites provide the dehydration of EG, thus completing the cascade reaction. Intermetallic interactions between Ru and W furnish the reaction selectivity due to synergy. This catalytic system can be controlled in such a way that it promotes hydrolysis, retro-aldol

condensation, dehydration, and hydrogenation to yield ethanol, while suppressing the side reaction such as oligomerization leading to humins.

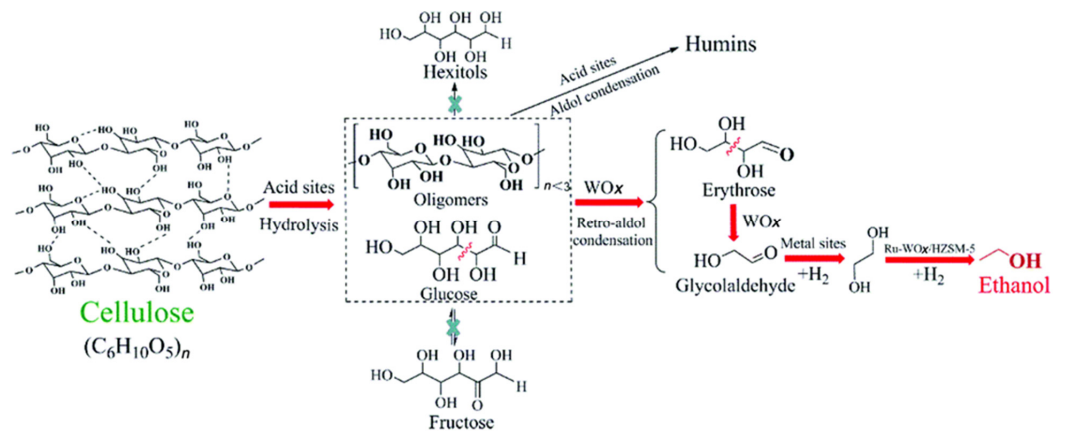


Figure 5. Reaction routes of cellulose conversion to ethanol over the Ru- WO_x /HZSM-5 catalyst. Reproduced with permission from [20] the Royal Society of Chemistry, 2019.

Zhao et al. reported a novel method of fixing Pt atoms incorporated in CeO_2 NPs inside the ZSM-5 structure for the catalytic transformation of FAL to CPO with the 97.2% selectivity at >99% conversion (Figure 6) [86]. In this catalyst, ultra-small CeO_2 NPs were placed on the surface of silica (S-1), which was further slowly transformed to ZSM-5, resulting in a multilayer structure with small Pt NPs obtained by impregnation. The authors determined that the advantage of this catalyst compared to the traditionally made analog is due to encapsulation of metal species into metal oxide and zeolite, which enhances metal-acid interactions.

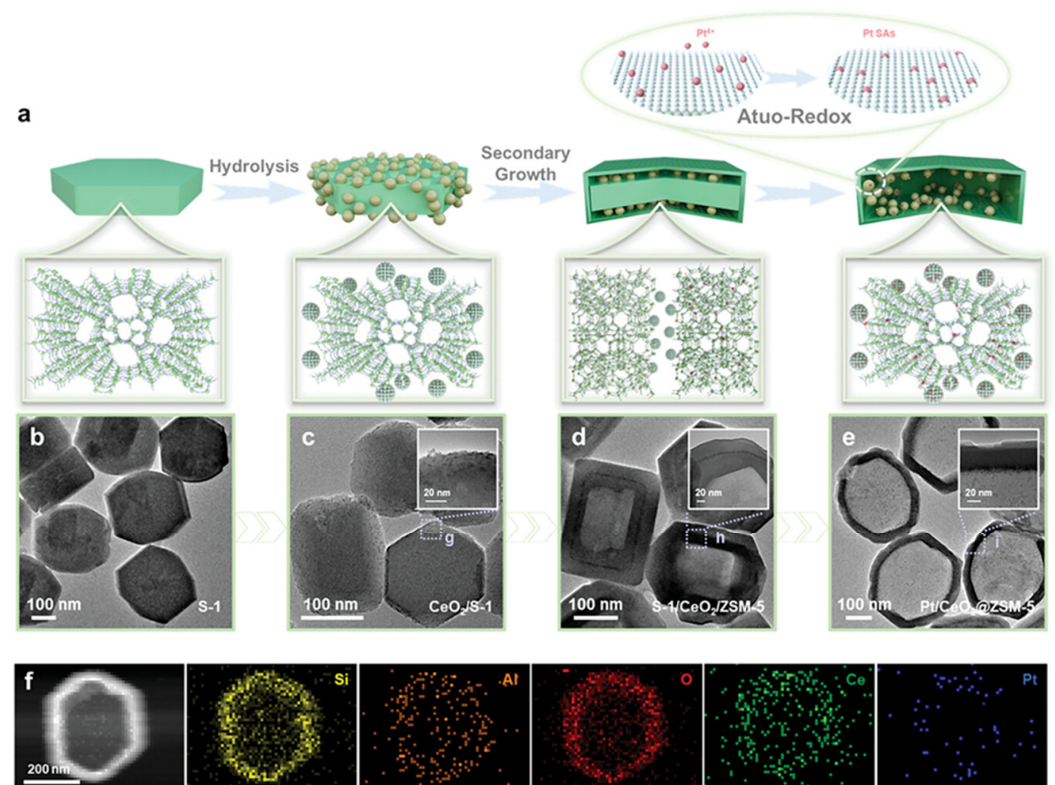


Figure 6. (a) Schematic illustration of the formation process of Pt/ CeO_2 @ZSM-5. TEM images of (b) S-1 (silica), (c) CeO_2 /S-1, (d) S-1/ CeO_2 /ZSM-5, and (e) Pt/ CeO_2 @ZSM-5. (f) STEM image and corresponding EDX mappings of Pt/ CeO_2 @ZSM-5. Reproduced with permission from [86] Wiley, 2024.

Porous carbons can be functionalized with carboxyl and hydroxyl groups during the pyrolysis of the precursor. These functionalities combined with metal sites create a multifunctional catalyst. In addition, when merged with zeolite, the catalyst can be beneficial for cascade reactions. A mixture of BEA and NiCu/C was utilized for the transformation of xylose (from biomass) to 2-methylfuran (MF) in a one-pot reaction [87]. BEA catalyzes the first step of the xylose transformation to FAL, while FAL to MF is converted over the bimetallic catalyst. Although zeolite here is not carrying an additional functionality, its presence allows for a significant increase of the reaction yield.

2.6. Zeolite Porosity

For multifunctional catalysts based on zeolites, the pore size of zeolites plays an important role in cascade reactions, whose course could be altered by a different mass transfer of reactants and products of different sizes [71,88,89].

2.6.1. Size and Morphology of Micropores in Zeolites

Different types of zeolites possess different pore sizes and pore structure, as was discussed in Section 2.1. Both parameters are crucial for the mass transport of reacting molecules, intermediates, and target products, thus providing selectivity for certain substances by allowing for intermediates to reach reactive sites or to be filtered out. In ref. [88], the authors used an original strategy encapsulating Pt NPs (with a mean diameter of 6 nm) using a cationic polymer, poly(diallyl dimethylammonium chloride) (PDDA), in MFI and BEA zeolites. These catalysts showed high efficiency in controlling the sequence of interactions of reagents and intermediates with different types of active sites. It was found that the change in the zeolite pore size is an efficient way to control selectivity in cascade reactions with bulky intermediates and products. Pt NPs encapsulated in H-BEA (pore size of 0.75 nm) (Pt@H-BEA) can catalyze a one-step conversion of CPO obtained from biomass to cyclic hydrocarbons C₁₀ (bicyclopentane and decalin) with a total yield of 78%. On the other hand, Pt NPs encapsulated in MFI with a micropore size of 0.56 nm and a similar density of metal and acid sites produced mainly cyclopentane (~70%). The kinetic analysis showed that the difference in the pore size between these two zeolites is the major cause of a dramatic change in selectivity, probably due to the higher energy barrier for the formation and diffusion of larger molecules. Pt-NPs deposited (not encapsulated) on H-BEA or H-ZSM-5 are not selective towards C₁₀ cyclic hydrocarbons in the CPO conversion, which highlights the importance of the architecture of the composite catalyst.

Ru NP-containing HZSM-5 catalysts displayed comparatively high selectivity in hydrogenolysis [29]. Here, three HZSM-5 zeolites with cross-shaped, spherical, and cuboid architectures with similar Si/Al ratios were explored in the development of Ru catalysts for guaiacol hydrogenolysis to benzene occurring in a cascade reaction through the guaiacol to phenol and then phenol to benzene transformations. For all three matrices, the Ru loading was ~5 wt.%, resulting in NP sizes in the range of 4–5 nm. The authors discovered that for cross-shaped HZSM-5, benzene was obtained with a 97% yield. The other two supports did not show selectivity. It was determined that the cross-shaped HZSM-5 possesses high mesoporosity and allows for the formation of well-defined NPs with a narrow NP size distribution. Moreover, the interaction between Ru NPs and HZSM-5 results in two types of Ru: electron-deficient and electronegative. Another important factor was the adsorption of larger amounts of guaiacol and hydrogen on the cross-shaped HZSM-5 surface. All these factors provided the highly selective catalyst, which, according to the authors, can be promising in the selective hydrogenolysis of biomass aliphatic compounds with C-O groups to their aromatic analogs.

The HDO of biocrude oil was carried out with Ru NPs based on four zeolites—BEA, HZSM-5, H-Y, and SAPO-34—whose pores differ by size and shape [78,79]. The Ru catalysts based on BEA and H-Y showed higher yields of MP than that for HZSM-5. This is consistent with larger pore channels in BEA and H-Y formed by 12 × 12 rings as compared to those in HZSM-5 (10 × 10 rings). The SAPO-34 based catalyst was the worst, which could be

explained by smaller pores due to eight-membered rings. A similar result was obtained by other authors in the reaction of C_6 sugars to FAL where the least selective catalyst was based on HZSM-5 with smaller pores [90]. The above data demonstrate that a mass transfer (diffusion), depending on the zeolite morphologies, is a very important factor in many catalytic (and especially cascade) reactions [71].

2.6.2. Mesoporous and Hierarchical Zeolites

Another step in enhancing or modifying the reaction outcome is the development of mesoporous (pore diameter of 2–50 nm) or hierarchical zeolites, i.e., zeolites with both micro- and mesopores (or macropores, >50 nm in diameter) [37]. The examples of the multifunctional catalysts based on mesoporous or hierarchical zeolites are numerous, so here, we will discuss only a few.

Bai et al. synthesized a meso/microporous lamellar Sn/Al catalyst based on MFI with LAS (Sn and Al) and BAS (Al-O(H)-Si) [12]. The catalytic reaction of choice was the glucose transformation to EMF, which is a three-step reaction. The first step is the isomerization of glucose to fructose carried out on Sn LAS, followed by the dehydration of fructose to HMF. The last step is the etherification of HMF with ethanol to form EMF on Al-O(H)-Si BAS. Crosstalk between several acid sites in an individual zeolite facilitated a one-pot cascade reaction of the carbohydrate transformation. The twofold porosity enabled an efficient mass transfer and facilitated the reaction steps.

A one-step transformation of cellulose to methyl lactate (MLA) and methyl 2-methoxypropionate (MMP) using a bifunctional catalyst—Zn-containing FAU (Y) modified by Ga—was carried out in supercritical methanol (scMeOH) (Figure 7) [91]. This zeolite, called nano-zeolite (HNZY) by the authors, was chosen because of a combination of micropores and large mesopores (10–30 nm) providing a high specific surface area and allowing easy access for such bulky molecules as cellulose and lignocellulose. Ga-ZnO NPs measured 3–7 nm and were well dispersed in HNZY. The increase in LAS and decrease in BAS were explained by the addition of Ga to ZnO. Optimal acidity along with the high surface area provided selectivity of the cellulose conversion. In optimal conditions, MLA and MMP were obtained with 70.6% yield when Ga doping was 1.8 wt.% and Zn loading was 9.8 wt.%.

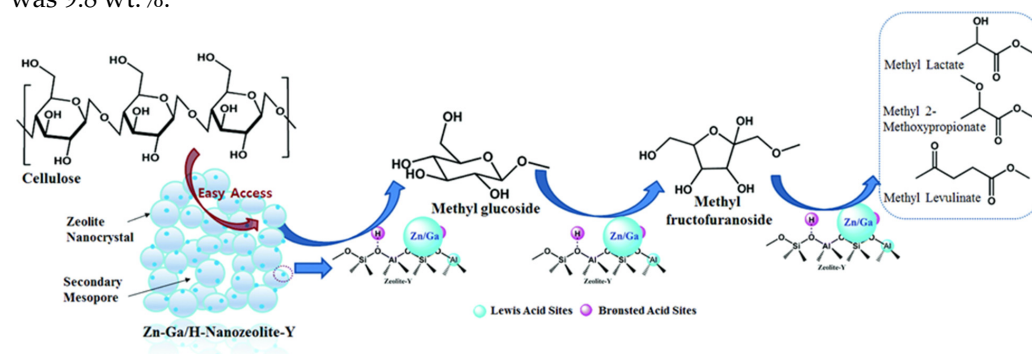


Figure 7. Proposed mechanism for the conversion of cellulose conversion to the major liquid products over Ga-doped Zn/HNZY in supercritical methanol. Reproduced with permission from [91] the Royal Society of Chemistry, 2017.

The other examples of zeolite-based catalysts with hierarchical porosity include Zr-Al-BEA [92] for the transformation of FAL to γ -valerolactone (GVL), ZrP catalysts for the conversion of FAL obtained from biomass to isopropyl lactate and GVL [16], and FAU based catalysts for the esterification pretreatment of bio-oil [93].

The other way to obtain variable porosity is to use a catalyst mixture. Tang et al. developed acid–base catalysts based on SAPO-11 with different Si/Al ratios and Zr-SBA-15 (mesoporous silica framework) with different Si/Zr ratios. Combined with Raney Ni, this catalyst mixture was efficient in the transformation of phenol by a cascade reaction, mimicking the pyrolysis oil conversion [25,94].

3. Catalysts Based on Mesoporous Solids

Mesoporous solids include metal oxides, silica, phosphates, carbons, and other materials. They may contain various acidic and basic sites which are, in combination with metal NPs, metal atoms, functional groups, etc., could be efficient multifunctional catalysts for cascade reactions. In this section, we will discuss the most important aspects of such catalysts that furnish their catalytic activity and selectivity.

A combination of one metal with another or with metal oxide can lead to an enhancement of redox properties due to a synergetic influence of metals which promotes electron transfer at the interface [37,95–97]. The efficiency of such a catalyst significantly depends on the composition and geometry of its surface. Subtle tuning of the energy distribution and electronic structure of the surface could control the activation energy barrier and determine the activity/selectivity of the catalyst [37]. For the targeted catalyst modification, several approaches dealing with electronic or geometrical surface structure were proposed [98]. The interactions between metal species and functional groups of the support can also result in property enhancement.

3.1. Influence of BAS/LAS or Basic Sites

As was discussed above for zeolite-based catalysts, the ratio and strength of acidity/basicity are crucial in many reaction steps and could determine the outcome of cascade reactions. The acidic properties can be varied by using (i) different loadings of the catalyst components, in particular, metal oxides incorporated into mesoporous silica [17], (ii) by phosphonation of activated carbons [99], or (iii) by controlling the type and strength of BAS and LAS on porous carbons [100]. Maderuelo-Solera et al. doped large silica spheres with varying amounts of ZrO_2 (with the Si/Zr ratio between 2.5 and 30) for the transformation of FAL to *i*-propyl furfuryl ether, *i*-propyl levulinate, and GVL via furfuryl alcohol (FOL) (Figure 8) [17]. If the Zr loading is low, the Zr species are evenly distributed in the silica spheres. In the case of the larger Zr loading, there is a segregation of ZrO_2 species into clusters. With the increase in the Zr loading, the ratio of LAS/BAS increases. Because LAS favor catalytic transfer hydrogenation (CTH) with alcohol as H-donor, while BAS facilitate dehydration, the LAS/BAS ratio changes the yield of reaction products [18]. A similar approach, i.e., the formation of ZrO_2/SiO_2 catalysts with LAS and BAS, was also reported by other authors for the transformation of FAL to GVL [18] and for the cascade conversion of biomass glucose to HMF [101]. Comparatively weak BAS and strong LAS along with surface hydrophobicity in mesoporous Zr-SBA-15 were favorable for the transformation of cellulose directly to ethyl lactate (EL) in a supercritical mixture of ethanol and water [102].

Shinde et al. developed a novel approach by mixing of two catalysts, Zr-Mont (Mont stands for montmorillonite) and $ZrO(OH)_2$, for the synthesis of high quality 2,5-bis(alkoxymethyl)furan via consecutive etherification, hydrogenation, and etherification again in a one-pot reaction (Figure 9) [103]. This catalyst mixture clearly demonstrates the importance of different acid sites for the efficiency of the reaction. BAS of Zr-Mont protonate the hydroxyl group in HMF with the formation of ether. At the next step, ether undergoes MPV reduction, which takes place on $ZrO(OH)_2$. Finally, alcohol formed by CTH participates in etherification with 2-propanol over Zr-Mont, leading to 2,5-bis(isopropoxymethyl)furan. Thus, the combination of a certain number of BAS and LAS, which could be controlled by the individual catalyst loading, determines the reaction outcome.

A different catalyst mixture consisting of two Zn-containing carbon-based catalysts was proposed for the cascade reaction of fructose to EL [104]. Depending on the Zn precursor, the catalyst contained either $Zn_5(OH)_8Cl_2 \cdot H_2O$ as active site or $Zn(OH)_{1.48}F_{0.52}$. The variation of these species allowed for the control of basic and acidic sites, resulting in the 78.2% yield and 98.2% total selectivity to EL.

A non-trivial approach to create LAS in mesoporous silica (TUD-1) was utilized by introducing Ni during silica formation [105]. An additional incorporation of Pd species resulted in the bimetallic Pd-Ni TUD-1 catalyst employed for a cascade reaction of FAL to 4-oxopentanal, MF, 2-alkoxyfuran, and acetals. The variation of acidity and the interaction

between metal and acid sites controlled the reaction products. The different roles of BAS and LAS were well assessed in the cascade reaction of DMF and ethylene to PX for the $\text{ZrO}_2/\text{SBA-15}$ catalysts modified by phosphate (H_3PO_4) [106]. The phosphate doping resulted in the zirconium phosphate and a large number of BAS, which increased the adsorption of reagents, leading to the intensification of the catalytic reaction. Moreover, the authors demonstrated that DMF was adsorbed and activated on BAS of P-OH. After that, ethylene adsorbed on LAS of Zr^{4+} and participated in the Diels–Alder reaction with DMF to produce a cycloadduct intermediate.

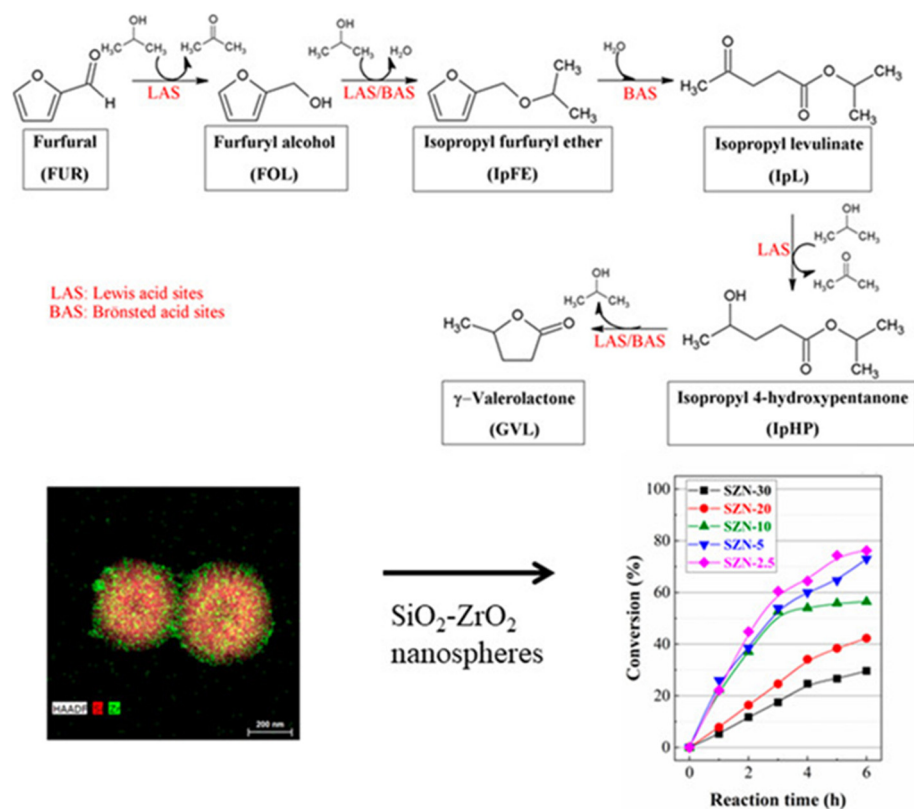


Figure 8. Reaction steps of furfural to GVL in the cascade reaction with $\text{SiO}_2\text{-ZrO}_2$ nanospheres. Reprinted without permission (CC-BY-4.0 license) from [17] the American Chemical Society, 2021.

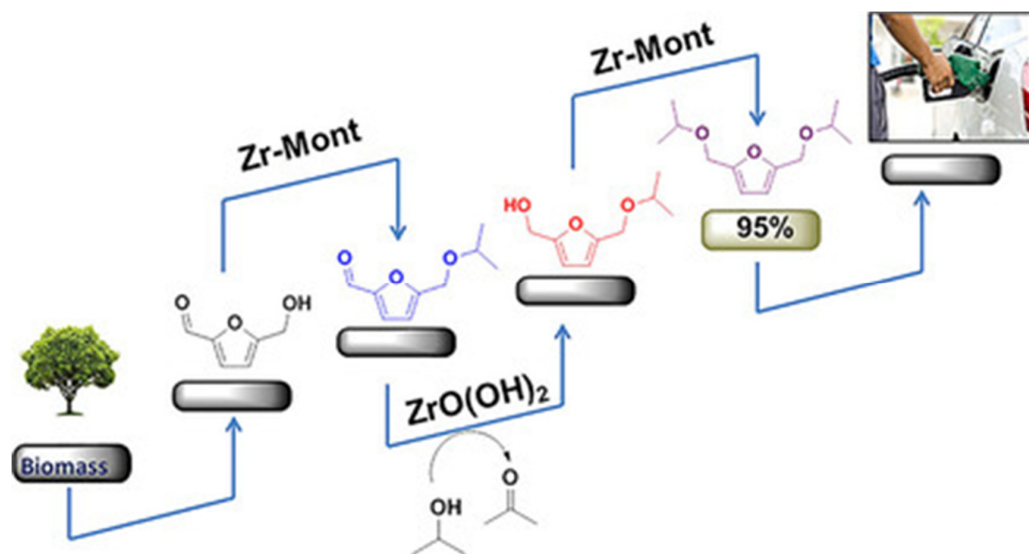


Figure 9. Schematic representation of the cascade reaction with the mixture of **Zr-Mont** and **ZrO(OH)₂**. Reproduced with permission from [103] from Wiley, 2017.

An abundance of BAS and LAS is found in heteropolyacids (HPA), also called polyoxometalates, which are assembled from various cations and anions into multifunctional clusters [107–109]. For example, a bifunctional HPA framework resembling zeolites was self-assembled from such ligands as organic pdc^{2-} (pyridine-2,6-dicarboxylate)[−], La^{3+} , WO_4^{2-} , and MoO_4^{2-} in hydrothermal conditions [108]. An optimal Brønsted acidity is considered to be the most influential factor in the HPA catalyst synthesized from choline chloride and $\text{H}_3\text{PW}_{12}\text{O}_{40}$ [109]. The HMF yield of 75% at the 87% conversion was obtained for the direct transformation from cellulose, which is quite a remarkable accomplishment. The authors ascribed this result to the combination of BAS, hydrophobicity, and other factors preventing further transformations of HMF. Zhang et al. discovered that monosubstituted phosphotungstic acids with the formula $\text{H}_n\text{PW}_{11}\text{MO}_{39}$, where M stands for the metal ion (Cu^{2+} , Zn^{2+} , Cr^{3+} , Fe^{3+} , Sn^{4+} , Ti^{4+} , and Zr^{4+}) can be excellent catalysts for a direct transformation of cellulose to methyl levulinate when the BAS/LAS ratio is equal 2.84/1 [107]. Moreover, the metal can be also crucial in influencing LAS and total acidity.

3.2. Support Porosity

The support porosity is a well-established factor influencing catalytic reactions. Nevertheless, for multifunctional catalysts based on mesoporous supports, there are hardly any papers with a systematic analysis of the porosity impact on catalysis. We believe this seeming shortcoming is due to the complexity of both multifunctional catalysts and cascade reactions. A good example is represented by ref. [110], where the authors studied Cu-containing catalysts formed from hydrotalcite (a layered magnesium–aluminum hydroxycarbonate) precursors. Changing the Cu compound loading, the pore size was varied in the range of 2–50 nm. However, the oxidation state of Cu species also changed, making it difficult to discern the clear dependence of the catalytic efficiency on either parameter. The best results in the transformation of FAL to MF where methanol was used as hydrogen donor (and solvent) were obtained for Cu_2Al with an average pore size of 7.9 nm and prevailing Cu^{2+} species. Similar results on the combined acid site and mesopore size influence (without understanding of the relationship for a single factor) were reported in ref. [111].

Saravanan et al. came as close as possible to singling out the porosity influence, although the second factor—acidity—was codependent [102]. The authors demonstrated that in mesoporous zirconium phosphates (*m*-ZrP), the larger pores containing a greater number of BAS and LAS were more favorable for the transformation of glucose to HMF than the smaller pores.

3.3. Metal NPs

Common knowledge is that the higher the dispersion (the smaller the NP size), the higher the catalyst activity. An excellent efficiency of the catalyst with low dispersion (large NP size) appears surprising if one considers only hydrogenation [22]. Indeed, it was demonstrated that large metal NPs lead to low activity in hydrogenation of cycloalkene [31], although earlier works demonstrated a hydrogen spillover decrease for smaller NPs [112,113]. Gabriel et al. reported a cascade reaction of menthol (from biomass) dehydration on acid sites and cycloalkene hydrogenation on noble metal NPs (Pt, Pd, and Ru) to target cycloalkanes on NP/ Nb_2O_5 [22]. Here, the larger NPs yielded the better result in dehydration (the rate determining step [23]) due to higher accessibility of the niobia acid sites, increasing the menthol conversion and resulting in the better total activity.

At the same time, the authors discovered that for Pt NPs deposited on Nb_2O_5 (several supports were tested), the small size of NPs (controlled by the Pt loading) is the most crucial parameter in the successful transformation of biomass-derived LA to N-substituted pyrrolidone (Figure 10) [33]. In particular, the best catalytic performance was observed for 0.2Pt/ Nb_2O_5 and 0.5Pt/ Nb_2O_5 , which produced Pt NPs with diameters of 0.6 nm. This was explained by the easy hydrogenation of small NPs. Niobia showed the best activation of C–O bond in LA (compared to other oxides), thus resulting in the 96% yield of 5-methyl-N-phenyl-2-pyrrolidone.

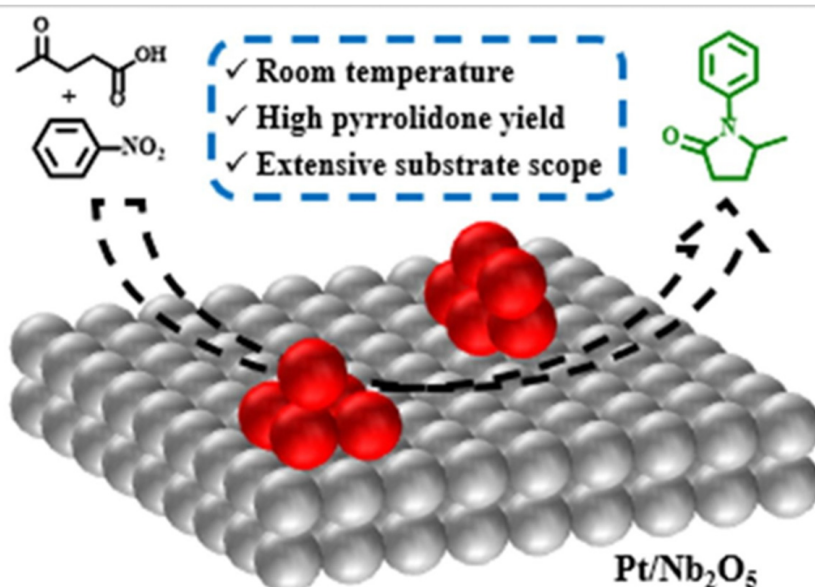


Figure 10. Schematic representation of Pt/Nb₂O₅ in hydrogenation and reductive amination of biomass-derived levulinic acid. Reproduced with permission from [33] Elsevier, 2024.

Similarly, small Pt NPs (0.6 nm) on the surface of WO_x NPs (~2.5 nm) (the latter deposited on ZrO₂) allowed for intimate interactions between the species. This resulted in synergy between components of this catalyst promoting the formation of 1-hexanol from HMF [114]. The small NP sizes allowed one to control the preferable ratio of zero valent and oxidized species (Pt⁰/Pt²⁺ and W⁵⁺/W⁶⁺ were equal to 4.58 and 0.31, respectively) and, consequently, the BAS amount. Cu NPs on activated carbon with different oxidation states of copper allowed for the efficient transformation of biomass polyols to glycolic acid [115]. Small Ru NPs formed in the layered double hydroxide, Ni₁MgAl, allowed high efficiency in reductive amination of FAL to furfurylamine due to Ru NP actions and two aluminum species: Al_{4c} and Al_{6c} [116].

3.4. Metal Atom Incorporation

Doping of Co₂AlO₄ with Pt atoms yielded the efficient catalyst for HDO of HMF to DMF with the 99% yield and high turnover frequency [117]. A single Pt atom was fixed on the support surface due to bonding with the surface oxygen atom. Spectral methods proved synergy between a single Pt atom activating C=O adsorption and neighboring BAS for C-O dissociation. Both experimental studies and DFT calculations demonstrated that the rate-determining step is the cleavage of the first C-OH bond on Pt, while BAS accelerate the breakage of the second C-OH bond.

The incorporation of Zn species into mesoporous silica resulted in the efficient catalyst for the transformation of biomass carbohydrates to EL [118]. It was found that Zn species were crucial for managing acidic and basic sites, thus controlling the selectivity of the process. Sn-doped biochar obtained from biomass showed the promising catalytic performance in the cascade reaction of biomass to furoic acid via FAL [119].

3.5. Synergy Between Functional Sites

Synergy between different functionalities in multifunctional catalysts can be realized in various ways. Most frequently, synergy is created between metal and acid sites located in vicinity of each other. At the same time, when more functional (or non-functional) groups are added to the catalyst, the mechanism can be much more complicated. Shi et al. developed a bifunctional catalyst, Pd/Al₂O₃, which was modified by phosphonic acid (PA) containing methyl groups (MPA) for the transformation of cellobiose—a model compound of cellulose—to sorbitol [21]. This cascade reaction includes three major steps: the hydro-

genation of cellobiose, the hydrolysis of cellobitol, and the hydrogenation of glucose to sorbitol (Figure 11). The catalyst modification results in the pronounced metal–support interaction between Pd and Al_2O_3 , which is significantly enhanced by PA, leading to better H_2 spillover from Pd species to the Al_2O_3 carrier. The adsorption of H_2 and its dissociation on Pd is enhanced due to the higher PdO/Pd ratio to stimulate hydrogenation of cellobiose. In turn, hydrolysis is enhanced due to the increase of LAS on Pd/ Al_2O_3 -MPA. It is noteworthy that methyl groups on the support surface further promote the cascade reaction by preventing undesirable hydrogen bonding between the intermediate and the surface. Thus, the major synergetic effect comes from the strong interactions between multiple species.

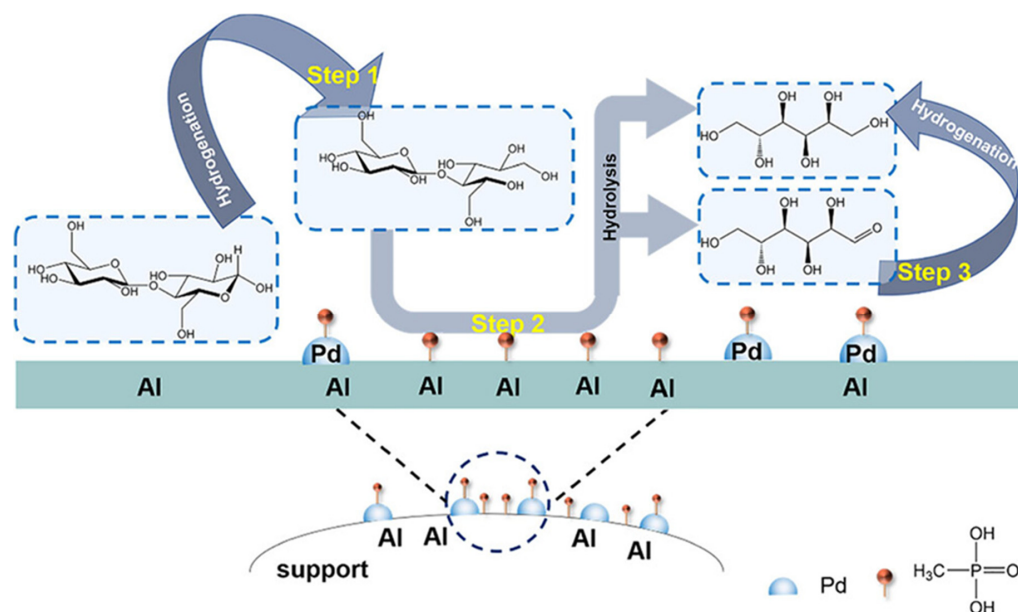


Figure 11. Conversion of cellobiose to sorbitol over Pd/ Al_2O_3 -MPA. Reproduced with permission from [21] the American Chemical Society, 2024.

CePO_4 nanorods were utilized as supports for deposition of Pd NPs for the cascade one-pot reaction of FAL with acetone to fuel precursors (Figure 12) [120]. The authors determined that the best results were obtained for the 3 wt.% Pd loading, which allowed for the most beneficial interactions between Pd and Ce species, thus enhancing the redox properties of the support and stimulating condensation and hydrogenation.

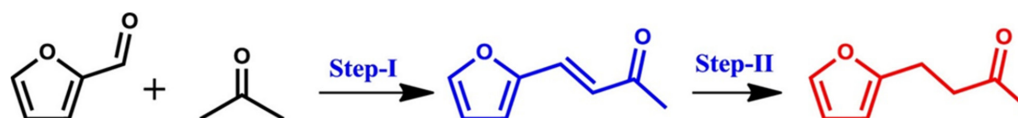


Figure 12. Schematic representation of the one-pot, two-step cascade reaction between furfural and acetone for the production of a C-C coupled hydrogenated product. Reproduced with permission from [120] the American Chemical Society, 2021.

The synthesis of 1,13-tridecanediol (TDOL) from biomass-based FAL is a complicated cascade reaction including several intermediates such as C_{13} difurfurylacetone (FAF) and 1,5-bis(furan-2-yl)-1,4-pentadien-3-one (HFAF) using HDO, hydrogenation, and ring opening (Figure 13) [121]. Such a complicated process required a non-traditional catalytic approach. This was achieved due to a mixture of two catalysts: Raney Ni and Pd/ TiO_2 - ZrO_2 (the latter with weak acid sites). The authors believe that the incorporation of a certain quantity of Pd in the TiO_2 - ZrO_2 support allows for controlling hydrogen adsorption and the strength of acid sites. Thus, the high selectivity of the TDOL synthesis is due to synergy between Pd and both oxides.

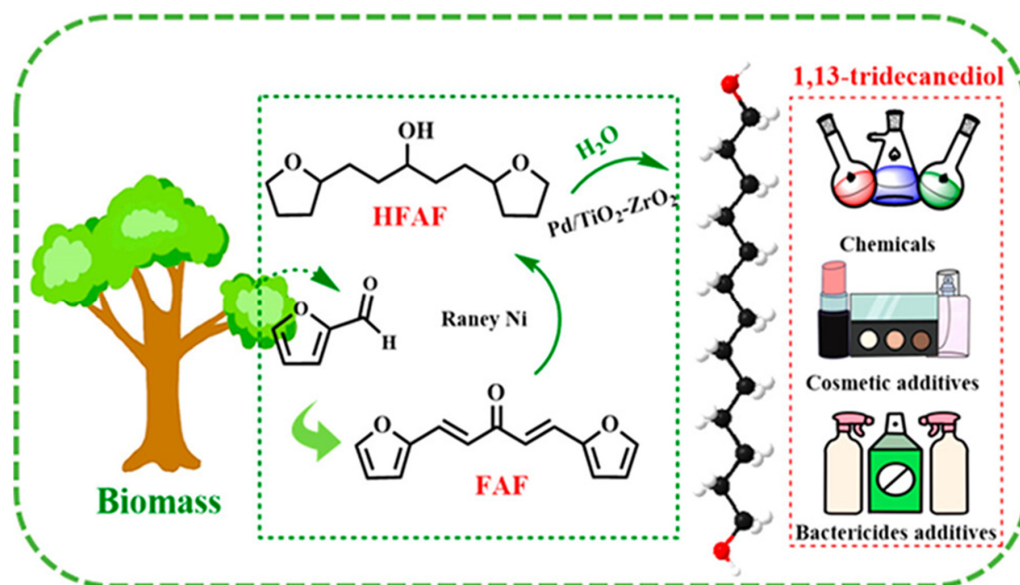


Figure 13. The formation of TDOL from HFAF on Pd/TiO₂-ZrO₂. Reproduced with permission from [121] the American Chemical Society, 2023.

Studying the Ru/Co₃O₄ catalysts, Liu et al. established that the relationships between the Ruⁿ⁺, Ru⁰, and oxygen vacancies in 1 nm Ru NPs are the key factors in successful syntheses of glyceric and glycolic acids from pentose [27]. A direct oxidation of glucose to glutaric acid (with tartronic and oxalic acids as coproducts) was investigated over bimetallic PtPd NPs formed on TiO₂ (Figure 14) [28]. A comparison of bimetallic and monometallic NPs showed that the former are significantly more efficient. In addition, the structure of bimetallic NPs plays an important role, with PtPd alloys being more favorable than the core-shell and cluster-in-cluster bimetallic structures. This indicates that the alloy structure provides the highest co-influence and synergy.

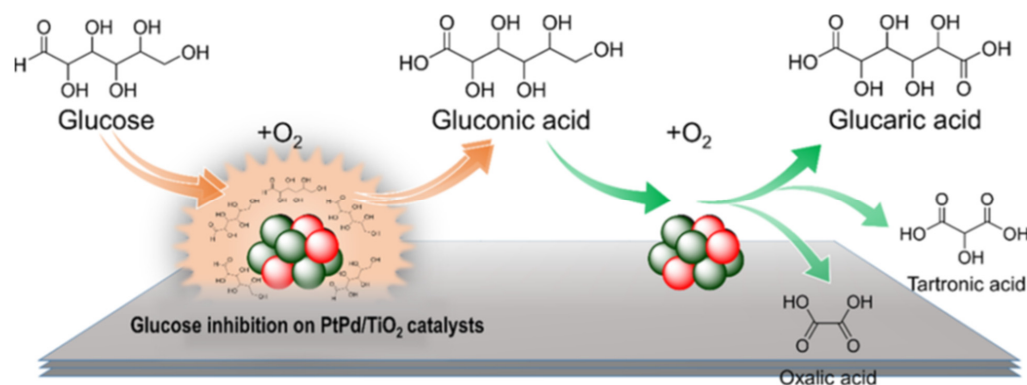


Figure 14. Direct oxidation of glucose with enhanced selectivity to gluconic acid with tartronic and oxalic acids as coproducts with bimetallic PtPd/TiO₂ catalysts. Reproduced with permission from [28] the American Chemical Society, 2016.

Similar results were observed in the cascade formation of GVL from biomass-derived reagents using an alloy of RANEY[®] nickel-tin deposited on aluminum hydroxide [122]. The high yield of the target compound over the RNi-Sn(x)/AlOH catalyst (x is the Sn amount) was assigned to synergy between two metals in the alloy structure and the acid groups of the support. In the case of Au NPs deposited on NiO, the synergistic effect was proposed for the interface between Au and NiO species [123]. This effect allowed for almost 92% conversion to C₇ and C₉ hydrocarbons with ~81% selectivity.

Synergy can be realized in metal-free catalysts, as is shown for carbon nanoplates treated with sulfuric and nitric acids (the latter leads to carboxyl groups) [124]. The co-influence of SO_3H and COOH groups as well as of unpaired electrons from the graphene sheet edge provides a synergistic effect in the fructose dehydration and HMF oxidation, resulting in 2,5-diformylfuran (DFF) with the 70.26% yield.

Quite unusual bifunctionality was discovered by Yu et al. when they incorporated sub-nanometer Ru clusters in porous carbon shells [125]. A charge transfer from Ru clusters to the curvature in carbon pores happened at the Ru/C interface and resulted in the metal-LAS bifunctional sites.

3.6. Catalyst Modification by Polymers with Acidic or Basic Groups

Modification with functional polymers is another way of the incorporation of multifunctionality into composite catalysts. Allegri et al. developed a novel catalyst using a spray-freeze drying technique and combining Aquivion (a copolymer of tetrafluoroethylene and ethanesulfonyl fluoride) and ZrO_2 for a one-pot transformation of FAL to GVL [19]. The authors determined that high activity and selectivity can be achieved by controlling the contents of BAS (from Aquivion) and LAS (from ZrO_2) via variation of the material composition.

Polymeric ionic liquids were also used for the preparation of hybrid catalysts [126,127]. Hou et al. fabricated bifunctional nanobelt type catalysts based on $\alpha\text{-CuV}_2\text{O}_6$ and mesoporous poly(ionic liquid) (MPIL) (Figure 15) for the direct transformation of fructose (biomass derived) to DFF [127]. A remarkable yield of DFF (>99.9%) was attributed to (i) the improved fructose adsorption on the hydrophilic polymer, (ii) the favorable adsorption and oxidation of the intermediate (HMF) on $\alpha\text{-CuV}_2\text{O}_6$, and (iii) the high activity of the Cu-O-V species.

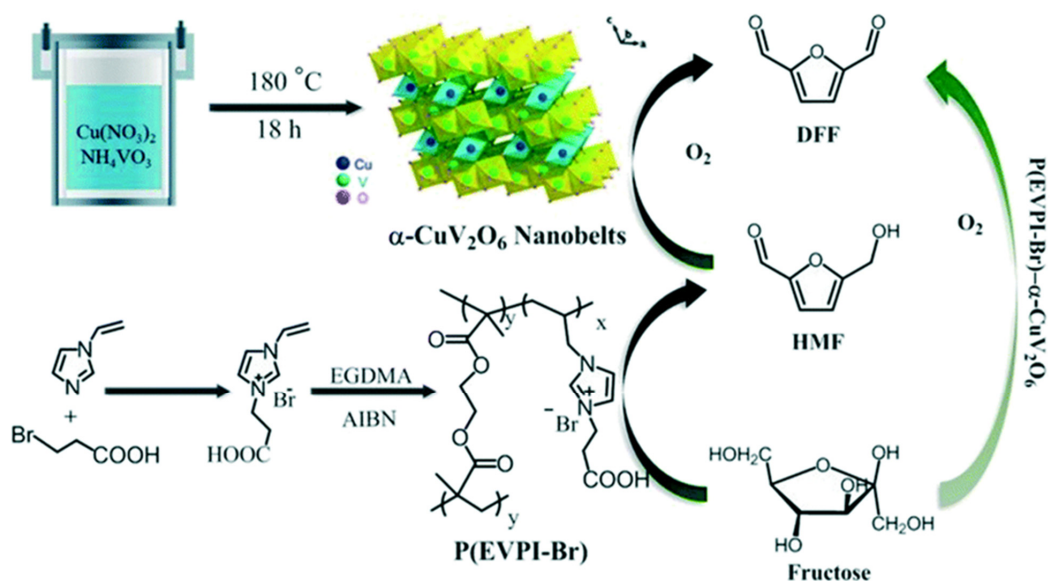


Figure 15. Synthesis of $\alpha\text{-CuV}_2\text{O}_6$ and MPIL P(EVPI-Br) for the conversion of HMF and fructose into DFF. Reproduced with permission from [127] the Royal Society of Chemistry, 2017.

3.7. Spatial Isolation of Metal and Acid Sites

The separation of acid and metal sites can be achieved when metal NPs are formed in the pores while functionalization occurs on the surface of porous solid [128,129]. An original solution to a complicated cascade reaction, i.e., a direct transformation of cellulose to 1,2-propylene glycol (1,2-PG) was proposed in ref. [30]. To control cellulose hydrogenolysis and to prevent side reactions due to high reactivity of intermediates, the authors proposed a yolk-shell nanoreactor made from N-doped carbon (NC) with Ru NPs (1.4 nm) and mesoporous carbon (MC) with acidic SO_3H groups, thus allowing for the site isolation of Ru and

acid species. A layer-by-layer method led to the NC core and the MC shell. Due to spatial separation of metal and acid sites in the Ru/NC@void@MC-SO₃H catalyst (Figure 16), the authors were able (i) to inhibit the poisoning of Ru NPs with SO₃H groups, (ii) to enhance the acid/base balance for the optimization of metal–acid interactions, and (iii) to furnish an improved diffusion pathway for preferred reaction species. The isolation of SO₃H groups in the magnetically recoverable Fe₃O₄@SiO₂@chitosan-SO₃H catalyst was also beneficial for the transformation of hexanedione and amines to N-substituted pyrroles [130,131] and for the synthesis of FAL from xylan in Al-modified activated carbon [132].

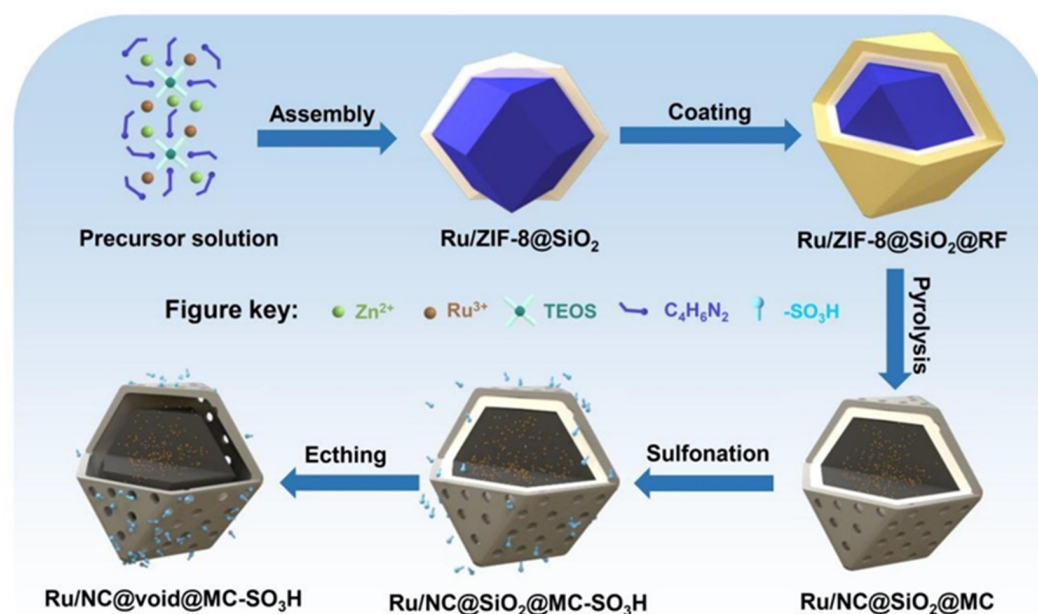


Figure 16. Schematic description of the synthetic process for Ru/NC@void@MC-SO₃H. Reproduced with permission from [30] Elsevier, 2023.

A surprising synergy was demonstrated by Garcia et al. in the catalyst mixture employed in the cascade transformation of FAL to GVL [133]. The mixture consisted of Pt NPs (1–2 nm) deposited on sepiolite (a hydrous magnesium silicate) and ZrO₂ NPs (~3 nm) deposited on a different batch of the same support. Remarkably, the catalyst mixture was found to be more efficient than the bimetallic Pt-Zr catalyst of the same composition, once again demonstrating that the spatial separation of active sites (Pt should stay in a zero valent state) can be beneficial in the multi-step catalytic process.

4. MOF-Based Multifunctional Catalysts

4.1. MOF Types

Metal–organic frameworks (MOFs) received considerable attention from the first report in 1995 [134] and were explored in numerous applications. MOFs are constructed from multivalent ions or clusters and rigid (normally aromatic) bifunctional linkers attached via coordination bonds [44,135–138]. Such an arrangement results in ordered porous structures, whose topology and morphology can be easily altered by varying the node nature and the type of the connecting ligand. Figure 17 shows typical MOFs.

MOFs possess extensive porosity as well as acidic, basic, and metal sites, which make them attractive in heterogeneous catalysis including biomass processing [13,137]. Below, we will discuss examples of the influence of the MOF structure on the catalytic performance in biomass relevant cascade reactions. As we indicated in preceding sections, cascade reactions require multiple functionalities. To achieve that, the MOFs presented in Figure 17 can be additionally functionalized with acidic or basic groups or their pores can serve as cavities for guest molecules or NPs, influencing the catalytic process.

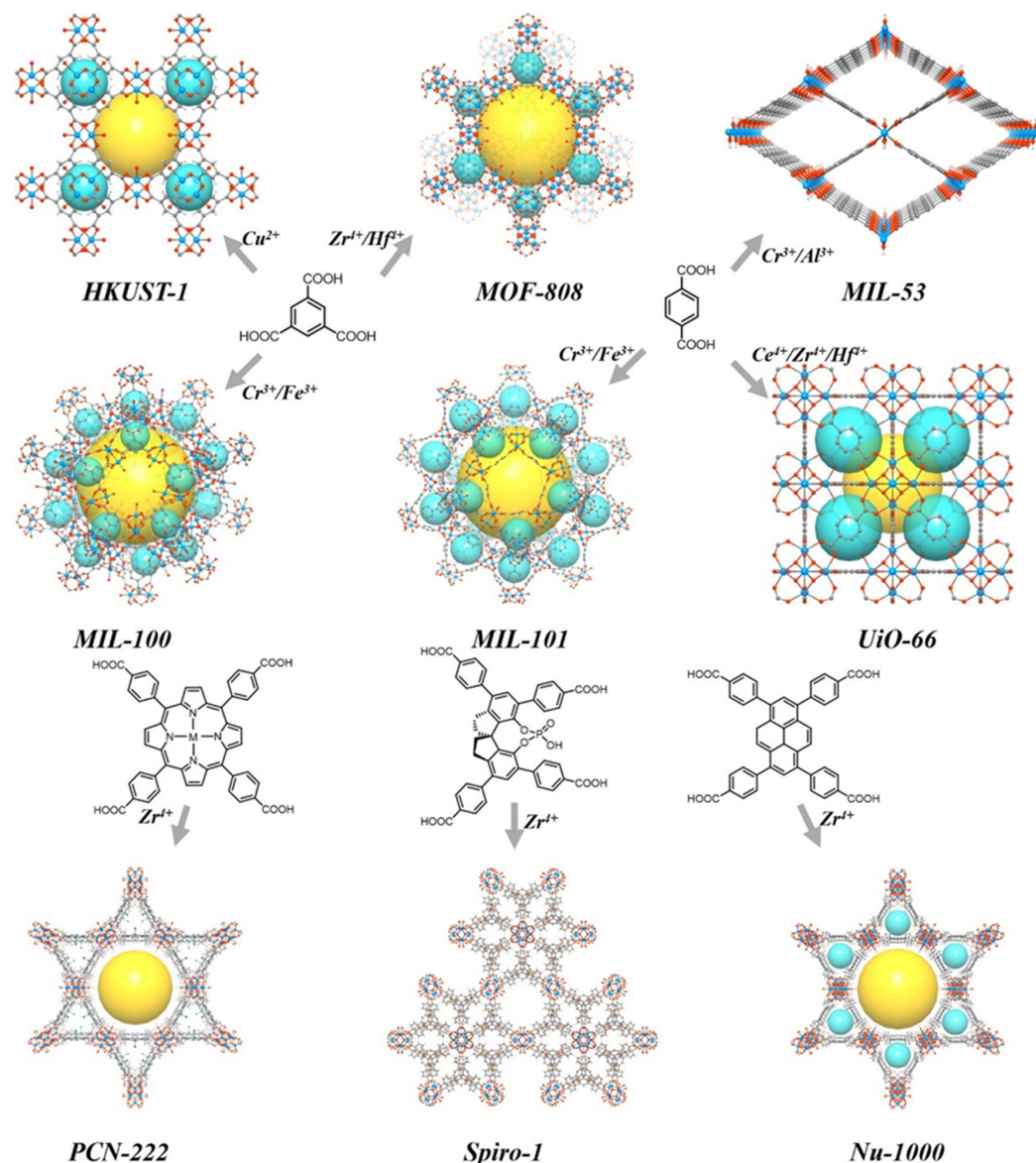


Figure 17. Typical MOF types with different active sites. Reproduced with permission from [135] Elsevier, 2020.

Most ubiquitous MOFs were developed by the Institute Lavoisier Frameworks and designated MIL [138]. They are typically formed by M^{3+} (where M is Cr, Fe, Al, V, Mn, etc.) terephthalates (benzene-1,4-dicarboxylates). The major MILs are MIL-47/MIL-53, MIL-88, MIL-100, and MIL-101, whose number stands for a specific structure [138]. By a modification of the linker with such groups as SO_3H , NO_2 , NH_2 , etc. (introduced during the MOF fabrication), acid and basic sites can be manipulated.

4.2. Functionalized MOFs

Sulfonated Zr-based MOF-808 containing both BAS and LAS were employed in the transformation of FAL to GVL [139]. A variation of the H_2SO_4 concentration used in the synthesis allowed one to alter the LAS/BAS ratio, leading to the 72.8% yield of GVL in optimized conditions. The same reaction was studied with sulfated DUT-67(Hf) using post-synthesis modification (Figure 18) [140]. Again, the catalyst acidity was varied by using aqueous sulfuric acid of different concentrations. The highest GVL yield of 87.1% was achieved with 0.06 mol/L aqueous sulfuric acid.



Figure 18. The structural transformation from pristine DUT-67(Hf) to DUT-67(Hf)-0.1SO₄. Atom labeling scheme: Hf, blue polyhedral; C, gray; O, red, S, yellow. All H atoms are omitted for clarity. Reproduced with permission from [140] Elsevier, 2019.

4.3. MOF Enhancement with Guest Molecules

MIL-101(Cr)-SO₃H containing both LAS and BAS was utilized in the transformation of biomass-derived glucose to HMF where the isomerization of glucose occurred on LAS and the dehydration of fructose to HMF happened on BAS [13,14]. However, the selectivity to HMF (depending on conditions) was moderate. The same reaction was considerably more efficient when MIL-101(Al)-NH₂ encapsulated a guest—phosphotungstic acid (H₃PW₁₂O₄₀, PTA)—adding BAS to the MOF catalyst [141]. The juxtaposition of BAS and LAS allowed for the synergetic effect and the higher activity and selectivity of the catalyst with the guest compound. A different MOF framework, MOF-808, was utilized for the impregnation with the same guest compound (here the authors used abbreviation HPW) and was successfully employed in the cascade transformation of LA to GVL with isopropanol as the hydrogen donor [142]. The highest GVL yield of 86% was achieved for an optimal HPW loading (14%) and was attributed to synergy between the available LAS from Zr⁴⁺ nodes and BAS from HPW. The former participate in the CTH, while the latter take part in the LA esterification with alcohol and lactonization to yield GVL. A schematic representation of HPW@MOF-808 is shown in Figure 19.

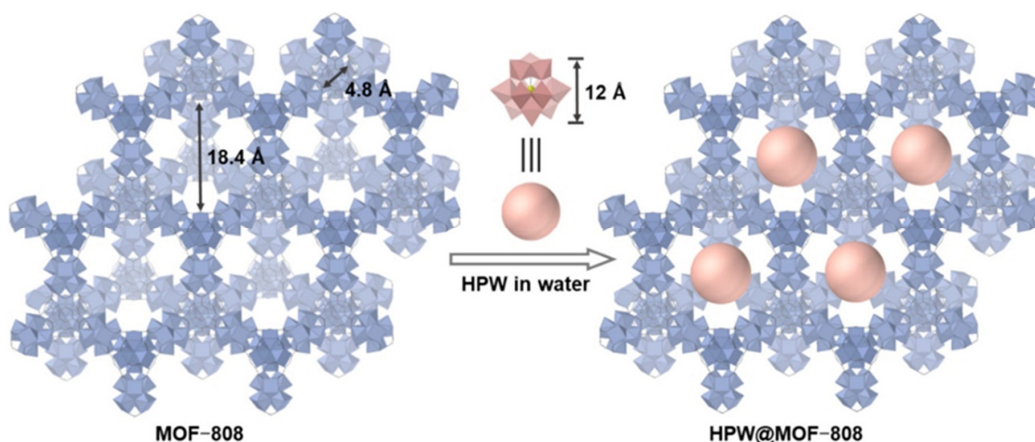


Figure 19. Synthesis of HPW@MOF-808 by a direct impregnation method. Reproduced with permission from [142] the American Chemistry Society, 2021.

The PTA incorporation in the MOFs formed by the $Zr_6O_4(OH)_4$ clusters as nodes (designated UiO) with additional Co species resulted in a promising catalyst for the conversion of fructose to 2,5-furandicarboxylic acid (FDCA) via HMF [143]. The catalyst designated PW/UiO(Zr, Co) (PW=PTA) led to the ~95% yield of FDCA (in the best reaction conditions) which was attributed to the optimal ratio of BAS/LAS from the incorporated species.

4.4. MOFs with NPs

Another important avenue for an enrichment of MOF properties for cascade catalytic reactions is the incorporation of metal NPs. Pd NPs with a mean diameter of 3.8 nm were prepared in MIL-101-SO₃H via thermal decomposition of Pd precursors and were well dispersed through MOFs [144]. This catalyst was explored in the transformation of furoic acid (FA, biomass derived) to ethyltetrahydro-2-furoate (ETF). Synergy between Pd NPs promoting hydrogenation and SO₃H sites catalyzing esterification results in an exceptional catalytic performance: nearly 100% conversion of FA and >99% selectivity to ETF.

Kulkarni et al. fabricated Pd NP-containing UiO-66 MOFs with Hf and Zr using two different approaches: (i) Pd NPs formed on the surface of MOFs and (ii) in the MOF framework given a core-shell structure [32]. The authors demonstrated that Pd@UiO-66 (Hf) (core-shell) displayed the best performance in the cascade transformation of FAL to furfuryl acetate due to surface acid sites and a cooperation between acid sites in the framework and Pd NPs. Ru NPs in sulfonated UiO-66 Ru catalyzed the transformation of ethyl levulinate (EL) to GVL [145]. Other UiO-66 substituents such as NH₂ and NO₂ slowed hydrogenation with Ru/UiO-66 to such a degree that the catalyst became inefficient in the cascade process.

4.5. MOF-Based Hybrid Catalysts

The polymers in hybrid catalysts based on MOFs can play several roles including the chemical and thermal stabilization of the MOF structure, the addition of multiple functional groups, and the creation of large pores, which are unavailable in MOFs. In ref. [146], the authors fabricated a macroporous polymer around UiO-66-SO₃H and UiO-66-NH₂ MOFs using a Pickering emulsion as template. This acid-base bifunctional catalyst was tested in the cascade reaction of cellulose to HMF and allowed 40.5% selectivity to the target product. Mesoporous polymeric organophosphate MOF-Hf, synthesized in situ and containing ~6.5 nm pores, has been utilized for the transformation of biomass-derived 4'-methoxypropiphenone to anethole (AN) [147]. A combination of the optimal BAS/LAS balance, low basicity, and high hydrophobicity allowed a remarkable AN yield of 98.9%.

A hybrid combining zeolite and MOF was constructed by growing UiO-66-NH₂ on the BEA surface and employed for the cascade reaction of sucrose to HMF (Figure 20) [148]. A combination of both catalysts increases the chemical stability of the hybrid catalyst, thus allowing for successful reusability. The exceptional 98% conversion with 100% selectivity for the catalyst containing 10% of BEA was attributed to multiple catalytic sites including BAS and LAS from BEA and MOFs and amino groups from UiO-66-NH₂, which successfully catalyzed each step of the cascade reaction.

It is noteworthy that despite that MOFs can be quite successful catalysts in numerous reactions, some authors prefer to use them as sacrificial templates to develop functionalized carbons. Cai et al. fabricated N-doped CuNi alloy carbons by the pyrolysis of bimetallic porphyrin MOFs for the transformation of FAL to CPO [149]. This approach allowed for smaller CuNi alloy NPs than conventional methods and the formation of N-Ni bonds, which assisted in hydrogenation and acid-catalyzed reactions, resulting in the 88.7% CPO yield.

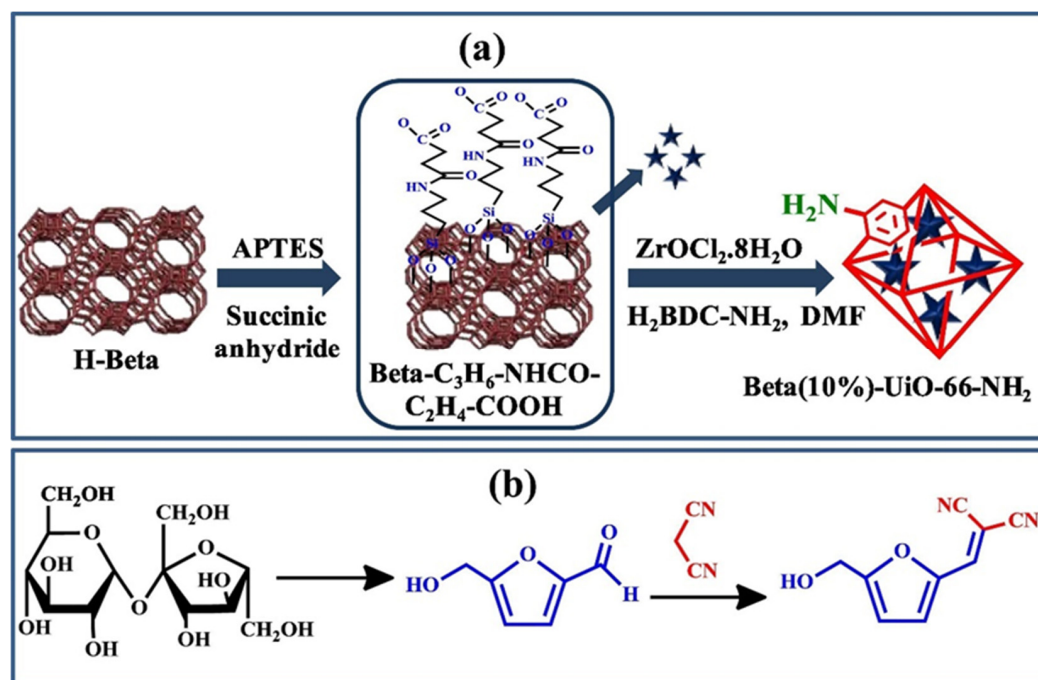


Figure 20. (a) Schematic representation for the synthesis of Beta(10%)-UiO-66-NH₂ nanocomposite, (b) One-pot, two-step conversion of sucrose to 2-((5-(hydroxymethyl)-furan-2-yl)methylene)malononitrile. Reproduced with permission from [148] Elsevier, 2019.

5. Metal NPs in N-Doped Carbon

Although the majority of porous solids is discussed in Sections 2 and 3, the catalysts based on N-doped carbon are assessed separately in this section because of the way bi(multi)functionality is created. Normally, the nitrogen doping of carbon is provided by using a pyrolysis precursor with nitrogen containing groups such as melamine [150–152], Zn₃[Co(CN)₆]₂ (Prussian Blue analog) [153], chitin [154], or ZIF-67 (zeolite imidazolate framework) [155]. N-doping plays an important role, allowing small, well-dispersed metal NPs due to interactions of nitrogen with the NP surface, altering the electronic structure of metal species, and creating surface oxygen vacancies, which are important in catalytic reactions [150]. Below, we will illustrate the catalysts based on N-doped carbons with a few examples.

Co-containing ZIF-67 (obtained in situ) was employed as a pyrolysis template to form Co NP containing N-doped carbon (Co@NHCS) (Figure 21) [155]. This catalyst was studied in the transformation of vanillin (from biooil) to 2-methoxy-4-methylphenol (MMP) biofuel, allowing one to achieve 100% conversion with 96% selectivity. Such successful HDO was explained by the enhanced electronic interactions of Co NPs and nitrogen species as well as the presence of multiple Co sites, activating reacting molecules and intermediates. In addition, the hierarchical porosity of these catalysts improved both NP stabilization and access to active sites.

Li et al. identified a dual role of hydrogen in the conversion of FAL to cyclopentanols with N-doped carbon containing Co NPs (Co@Co-NCs) [153]. The standard role of H₂ is a reducing agent in hydrogenation. Here, H₂ is also stimulating the reaction steps catalyzed by acids. Hydrogen causes a transfer from LAS to BAS (via heterolysis) in the N-doped carbon shell around Co NPs, involving water and leading to the cyclopentanol yield of >90% (Figure 22).

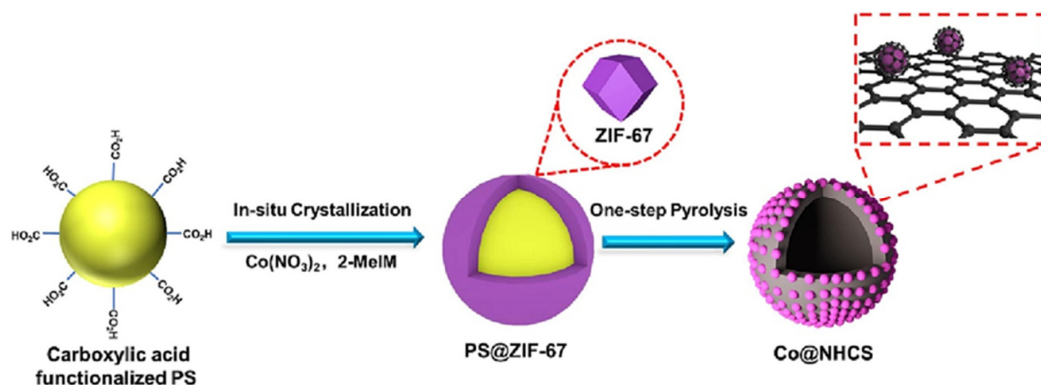


Figure 21. Schematic illustration for the synthesis of Co@NHCS nanocatalysts. Reproduced with permission from [155] Elsevier, 2023.

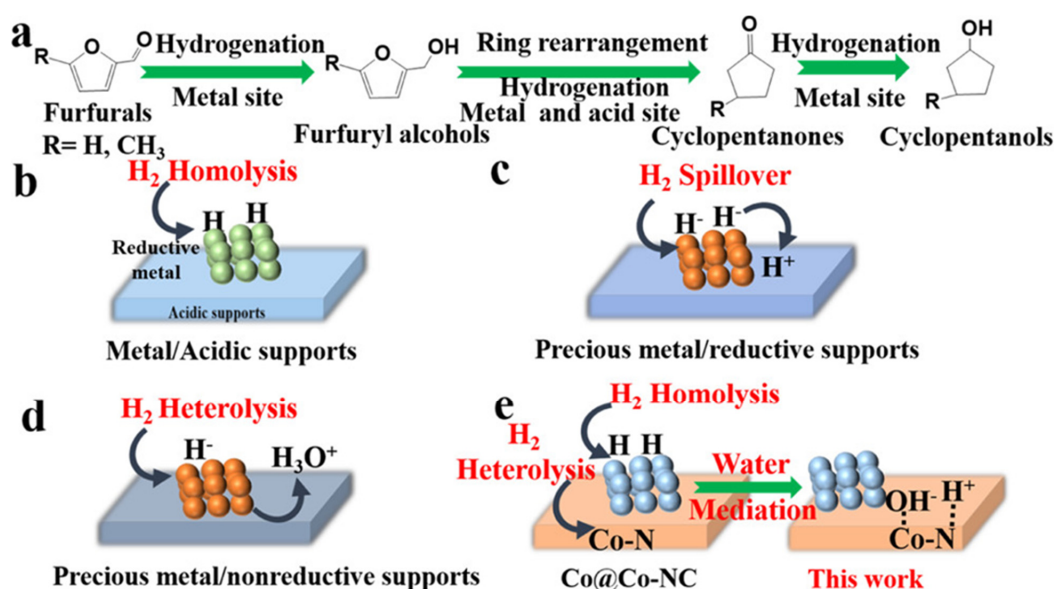


Figure 22. Hydrogenative ring rearrangement pathway of furfurals to cyclopentanols (a) and different bifunctional reaction mechanisms (b–e). Reproduced with permission from [153] the American Chemical Society, 2022.

In complex processes that start from true biomass, a bifunctional catalyst based on N-doped carbon can be insufficient. Park et al. developed a mixture of Pd NPs in N-doped carbon ($\text{Pd}_{0.1}/\text{CN}_x$) and Ni NPs on activated carbon coated with passivated alumina ($\text{Ni}_2@\text{Al}_2\text{O}_3/\text{AC}$) for the treatment of lignocellulosic biomass (birch sawdust) to polyols and monocarboxylic acids, although the yields were quite low: 21.6% and 7.9%, respectively [151]. Another complex catalyst (not a mixture) was reported by Parrilla-Lahoz et al. for the HDO of guaiacol to benzene using water as a hydrogen source [156]. The authors fabricated the catalyst consisting of Ni NPs placed on the surface of N-doped graphene with attached zirconia particles. Although the efficiency of this catalyst was moderate, it allowed one to eliminate the dangerous and expensive hydrogen normally used in this reaction.

6. Enzymatic Multifunctional Catalysts

Immobilized enzymes, i.e., enzymes attached to a support, were shown to be superior compared to native enzymes (utilized in solutions) in terms of increased thermal and chemical stability and reusability with the reasonable preservation of their enzymatic activity [157,158]. Several avenues have been explored for the fabrication of multifunctional enzymatic catalysts for cascade reactions in biomass processing [159–162]. Multifunctionality can be created by two or more enzymes, enzymes and acidic or basic groups, enzymes

and metal sites, etc. In heterogeneous catalysts, different functionalities can be immobilized on the same [163–170] or different supports [171]. In the latter case, the mixture of functionalized supports is used in a one-pot catalytic reaction. In both instances, there is a danger that the presence of strong acidic groups can deactivate enzymes, or that acidic groups are neutralized by enzymes, so a careful choice of catalytic sites is a paramount concern [172]. Immobilized enzymes are the answer to stability problems, although such an approach is not commonly used for cascade reactions involving biomass. Several reports described chemoenzymatic cascade reactions when a solid acid is combined with enzymes in solution [132,172–179] or when both acidic and enzymatic catalytic reactions were carried out with liquid catalysts [180,181]. The former approach can be illustrated by ref. [182], where a heterogeneous solid acid, sulfonated Al-Laubanite (a mineral), and native ω -transaminase are used in a sugarcane bagasse transformation to furfurylamine (FLA) in a deep eutectic solvent (ChCl:Gly-water) that, additionally, supplies BAS and LAS. In this reaction setup, sulfonated Al-Laubanite catalyzes a transformation to FAL, while the FLA synthesis is catalyzed by the enzyme in conjunction with ChCl:Gly-water.

In our opinion, these catalytic systems are not sustainable because they cannot be reused or used in continuous processes, but they do assist in biomass processing to value added chemicals. Arias et al. reported a chemoenzymatic transformation of HMF (biomass-derived) and carboxylic acids or esters to the diesters of 2,5-bis(hydroxymethyl)furan (BHMF), which serve as replacement plasticizers (Figure 23) [183]. In this cascade process, the first step (reduction in HMF to BHMF) involves Co NPs with a carbon shell, while the second step—esterification—involves immobilized lipase. The total yield of the final product reached ~90% and the continuous process was realized for at least 60 h. These data indicate, once more the advantages of heterogeneous catalysts in cascade reactions.

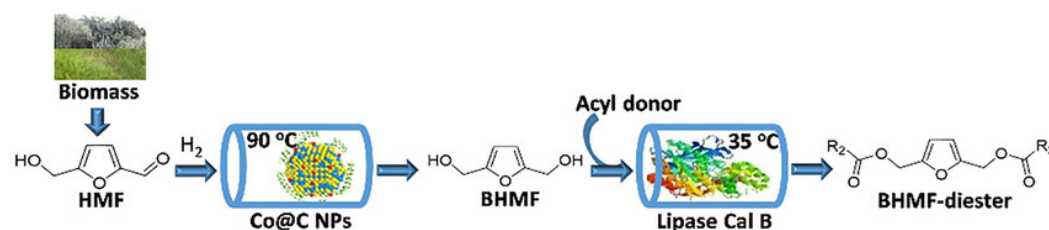


Figure 23. Pathway of the transformation of HMF and carboxylic acids or esters to BHMF. Reproduced with permission from [183] Wiley, 2020.

7. Catalyst Regeneration and Continuous Processes

The stable catalytic performance in cascade reactions is a crucial feature of multifunctional catalysts determining their possible practical applications. It can be improved by suitable regeneration when the catalyst efficiency diminishes. The major pathway of catalyst poisoning is blocking active sites with adsorbed carbonaceous materials. If the zeolite-based catalyst contains no thermally sensitive sites, it can be washed with alcohols (i.e., ethanol, methanol) and then calcined at 500–550 °C [15,106]. When noble metal species are present, they can be reduced with hydrogen at 400 °C to restore their valent state [88]. The catalyst based on a mesoporous oxide was regenerated by washing with methanol and drying in a vacuum at 80 °C [27]. In some cases, regeneration includes drying overnight at 110 °C followed by calcination at 450 °C [126]. Carbon-based catalysts are regenerated only in mild conditions by washing with methanol or ethanol and drying at 80–100 °C [100,130]. MOFs are normally washed (with deionized water, ethanol, or toluene) to remove carbonaceous deposits followed by vacuum drying at 80–150 °C (the temperature depends on the thermal stability of the framework) [13,14]. In the case of sulfated MOFs, acid regeneration can be carried out to restore acid sites [140]. The catalyst stability and ease of regeneration are especially essential in continuous processes.

The importance of continuous reactions can be hardly overstated because they pave the way for such reactions in industrial applications. To the best of our knowledge, there are only several examples of multifunctional catalysts utilized in the continuous

cascade processes, one of which was briefly discussed in the previous section [183]. Here, we are trying to analyze whether a special catalyst type is needed to be successful in continuous processes or whether there is merely a disconnect between scientists and engineers in developing such processes.

Wang et al. reported a one-pot preparation of 1,4-PDO from FOL in both batch and continuous conditions using a carefully chosen layered double hydroxides CuMgAl mix, obtained with mixed alkali precipitants [184]. In the batch process, the authors determined that for the best catalytic performance, the catalysts should possess an optimal ratio of acid and base sites and small Cu NPs with high electron density, which catalyzes the EL carbonyl group opening. In the continuous process, HZSM-5 was added in the fixed bed reaction for the first step (Figure 24). This resulted in the remarkable yield of 94.3% for the target product in the alcoholysis hydrogenation integrated cascade process.

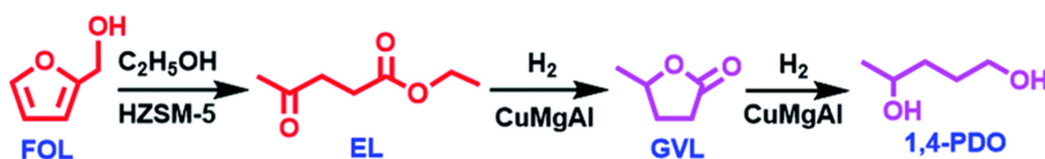


Figure 24. Preparation of 1,4-PDO through FOL alcoholysis and subsequent hydrogenation. Reproduced with permission from [184] the Royal Society of Chemistry, 2022.

A morphologically simple catalyst based on commercial titania with deposited 1 wt.% of Pt (small NPs invisible in TEM) was shown to display high activity (87% conversion) and great selectivity (>80%) for a continuous cascade transformation of LA to 1-ethyl-5-methylpyrrolidin-2-one via several steps [96]. Here, the combination of unobstructed porosity, stable acidity, and high activity of Pt species provides a successful outcome of the above reaction.

In Section 3.7 we discussed the benefits of the spatial separation of metal and acidic sites due to the placement of Pt NPs and ZrO_2 NPs on separate supports of the same nature to preserve the Pt zero valent state [133]. This catalyst showed a great performance in the batch process (the conversion of FAL to GVL), but selectivity went significantly down when the catalyst mixture was tested in the continuous process due to side reactions. It was not quite clear why this mismatch took place, emphasizing once more obstacles in transferring successful batch conditions and catalysts into continuous ones.

8. Conclusions

The data presented in this review article clearly show that the cascade reactions in biomass processing require bi- or multifunctional catalysts to optimize each step of the process and to allow a one-pot reaction setup. Depending on raw materials and target products, different catalysts need to be fabricated, considering their stability, acidity, metal site interactions, porosity, etc. For all the catalysts, the BAS/LAS ratio and strength are the crucial factors. In zeolites, they could be controlled by changing the Si/Al ratio during the synthesis or the post-synthesis treatment by desilication, dealumination, incorporation of other species, etc. When metal species are present, their interactions with acid–base sites often result in synergy, leading to the intensification of the reactions or the selectivity enhancement. The separation of active sites is another important path for catalyst improvement, allowing the preservation of active site integrity.

In zeolite-based catalysts, the pore size and geometry determine not only the activity and selectivity of the reaction, but also the type of the final product. Intermediates could be filtered out due to their size or shape, if they are incompatible with the pore channel. For the catalysts based on mesoporous materials, such clear dependences were not observed because the increase of the pore size and pore volume occurs simultaneously with the increase of BAS/LAS; thus, the porosity influence as a single factor cannot be elucidated.

Control of the product outcome with pore sizes and shapes and the easy manipulation of acidity are major advantages of zeolite supports. The key limitation is a poor mass

transfer if hierarchical porosity is not added. The catalysts based on mesoporous solids usually provide better transport of reactants and intermediates, but their multifunctionality requires more complex approaches to incorporate all active sites. In mesoporous carbons, N-doping provides additional advantages for the formation of small, well-dispersed metal NPs with the altered electronic structure and abundant surface oxygen vacancies, which are important in catalytic reactions. MOFs are appealing due to the simplicity of their syntheses via self-assembly, but they often need additional acid sites and are less chemically stable. Enzymatic catalysts are unsurpassed from the viewpoint of environmental benefits, but even immobilized enzymes can only function within a comparatively narrow temperature and pH range. Thus, hybrid catalysts combining several above-mentioned supports could be more beneficial in complex cascade reactions.

To better understand which catalyst feature plays the crucial role in the selectivity of the certain cascade reaction, we compared different catalysts in two transformations: (i) FAL to GVL and (ii) FAL to CPO. We assume that the reaction conditions are optimized, so we neglect this factor. In the case of Zr-Al-BEA (zeolite) with hierarchical porosity, the GVL yield reached 95% [92]. For sulfated DUT-67(Hf) (MOFs), the yield was 87.1% [140]. In both cases, BAS/LAS ratios and strengths were optimized and synergy was achieved. Both catalysts were nanostructured, allowing the optimal positioning of active sites. Both catalysts had similar surface areas, but Zr-Al-BEA possessed hierarchical porosity, while DUT-67(Hf) was microporous. Because hierarchical porosity facilitates mass transfer, it can be responsible for the increase in the GVL yield in this case. For the FAL-to-CPO process, the 98% CPO yield was achieved for 2% Pd/HZSM-5(25) [1], while for Ni-Cu-NPC-500 (bimetallic NPs in N-doped carbon), only the 88.7% yield was obtained [149]. For the former catalysts, BAS, LAS, and metal sites were optimized, as were interactions between functionalities. In the latter catalyst, there are no classical acid–base sites like in zeolites or metal oxides. In this case, $\text{OH}^{\delta-}$ -Ni-N- $\text{H}^{\delta+}$ bonds are formed, which are responsible for acid catalysis. We believe that it is most likely the acidic catalysis is not sufficiently optimized, decreasing the selectivity.

In Section 7 we assessed the possibility of continuous cascade processes, the studies of which are required for transfer of the accomplishments of the scientific community into industry. According to our analysis, the catalysts should be heterogenous, chemically, and thermally stable, and their active sites (including the metal oxidation state) should be preserved during a lengthy catalytic process. In addition, a suitable reactor design is as important as the excellence of the catalyst itself. In our opinion, a commercial development of this field depends on a close collaboration of scientists and engineers to implement the best catalytic solutions in suitable catalytic reactors.

Author Contributions: Conceptualization, writing—original draft preparation, and writing—review and editing, L.M.B. and V.G.M. All authors have read and agreed to the published version of the manuscript.

Funding: This work was funded by the Russian Science Foundation (project 23-79-00009).

Conflicts of Interest: The authors declare no conflicts of interest.

Abbreviations

BAS	Brønsted acid sites
BHMF	2,5-Bis(hydroxymethyl)furan
BV	Baeyer–Villiger oxidation
CPO	Cyclopentanone
CTH	Catalytic transfer hydrogenation
DMF	2,5-Dimethylfuran
EG	Ethylene glycol
EL	Ethyl lactate
EMF	5-(Ethoxymethyl)furfural
ETF	Ethyltetrahydro-2-furoate

FA	Furoic acid
FAF	Difurfurylacetone
FAL	Furfural
FLA	Furfurylamine
FOL	Furfuryl alcohol
GVL	γ -Valerolactone
HDO	Hydrodeoxygenation
HFAF	1,5-Bis(furan-2-yl)-1,4-pentadien-3-one
HMF	5-Hydroxymethylfurfural
HNZY	Nano-zeolite
LA	Levulinic acid
LAS	Lewis acid sites
MC	Mesoporous carbon
MF	2-Methylfuran
MLA	Methyl lactate
MMP	Methyl 2-methoxypropionate
MOFs	Metal-organic frameworks
MP	2-Methylpiperidine
MPA	Methyl phosphonic acid
MPIL	Mesoporous poly(ionic liquid)
MPV	Meerwein-Ponndorf-Verley
NC	N-doped carbon
NPs	Nanoparticles
OPO	Oppenauer oxidation
PA	Phosphonic acid
PDDA	Poly(diallyl dimethylammonium chloride)
1,4-PDO	1,4-Pentanediol
1,2-PG	1,2-Propylene glycol
PTA	Phosphotungstic acid
TDOL	1,13-Tridecanediol

References

- Gao, X.; Ding, Y.Y.; Peng, L.L.; Yang, D.; Wan, X.Y.; Zhou, C.M.; Liu, W.; Dai, Y.H.; Yang, Y.H. On the effect of zeolite acid property and reaction pathway in Pd-catalyzed hydrogenation of furfural to cyclopentanone. *Fuel* **2022**, *314*, 123074. [[CrossRef](#)]
- Bhanja, P.; Bhaumik, A. Porous nanomaterials as green catalyst for the conversion of biomass to bioenergy. *Fuel* **2016**, *185*, 432–441. [[CrossRef](#)]
- Kim, S.; Kwon, E.E.; Kim, Y.T.; Jung, S.; Kim, H.J.; Huber, G.W.; Lee, J. Recent advances in hydrodeoxygenation of biomass-derived oxygenates over heterogeneous catalysts. *Green Chem.* **2019**, *21*, 3715–3743. [[CrossRef](#)]
- Sun, Z.; Duan, X.; Gnanasekarc, P.; Yan, N.; Shi, J. Review: Cascade reactions for conversion of carbohydrates using heteropolyacids as the solid catalysts. *Biomass Convers. Biorefin.* **2022**, *12*, 2313–2331. [[CrossRef](#)]
- Zhong, R.; Sels, B.F. Sulfonated mesoporous carbon and silica-carbon nanocomposites for biomass conversion. *Appl. Catal. B* **2018**, *236*, 518–545. [[CrossRef](#)]
- Bayu, A.; Abudula, A.; Guan, G. Reaction pathways and selectivity in chemo-catalytic conversion of biomass-derived carbohydrates to high-value chemicals: A review. *Fuel Process. Technol.* **2019**, *196*, 106162. [[CrossRef](#)]
- Li, S.; Deng, W.; Wang, S.; Wang, P.; An, D.; Li, Y.; Zhang, Q.; Wang, Y. Catalytic Transformation of Cellulose and Its Derivatives into Functionalized Organic Acids. *ChemSusChem* **2018**, *11*, 1995–2028. [[CrossRef](#)] [[PubMed](#)]
- Liu, X.; Zhang, H.; Chang, F.; Huang, S.; Yang, K.; Yang, S. Catalytic Transformations of Organic Compounds and Biomass Derivatives with Functionalized Metal-Organic Frameworks. *Curr. Org. Chem.* **2016**, *20*, 761–776. [[CrossRef](#)]
- Sudarsanam, P.; Zhong, R.; Van den Bosch, S.; Coman, S.M.; Parvulescu, V.I.; Sels, B.F. Functionalised heterogeneous catalysts for sustainable biomass valorisation. *Chem. Soc. Rev.* **2018**, *47*, 8349–8402. [[CrossRef](#)] [[PubMed](#)]
- Xu, H.; Ju, J.; Li, H. Toward efficient heterogeneous catalysts for in-situ hydrodeoxygenation of biomass. *Fuel* **2022**, *320*, 123891. [[CrossRef](#)]
- Dijkmans, J.; Dusselier, M.; Janssens, W.; Trekels, M.; Vantomme, A.; Breynaert, E.; Kirschhock, C.; Sels, B.F. An Inner-/Outer-Sphere Stabilized Sn Active Site in β -Zeolite: Spectroscopic Evidence and Kinetic Consequences. *ACS Catal.* **2016**, *6*, 31–46. [[CrossRef](#)]
- Bai, Y.Y.; Wei, L.; Yang, M.F.; Chen, H.Y.; Holdren, S.; Zhu, G.H.; Tran, D.T.; Yao, C.L.; Sun, R.C.; Pan, Y.B.; et al. Three-step cascade over a single catalyst: Synthesis of 5-(ethoxymethyl)furfural from glucose over a hierarchical lamellar multi-functional zeolite catalyst. *J. Mater. Chem. A* **2018**, *6*, 7693–7705. [[CrossRef](#)]

13. Chatterjee, A.; Hu, X.J.; Lam, F.L.Y. Catalytic activity of an economically sustainable fly-ash-metal-organic-framework composite towards biomass valorization. *Catal. Today* **2018**, *314*, 137–146. [[CrossRef](#)]
14. Su, Y.; Chang, G.G.; Zhang, Z.G.; Xing, H.B.; Su, B.G.; Yang, Q.W.; Ren, Q.L.; Yang, Y.W.; Bao, Z.B. Catalytic dehydration of glucose to 5-hydroxymethylfurfural with a bifunctional metal-organic framework. *AIChE J.* **2016**, *62*, 4403–4417. [[CrossRef](#)]
15. Lodhi, A.; Maheria, K.C. Zeolite-catalysed esterification of biomass-derived acids into high-value esters products: Towards sustainable chemistry. *Catal. Commun.* **2024**, *187*, 106883. [[CrossRef](#)]
16. Ye, L.; Han, Y.W.; Bai, H.; Lu, X.B. HZ-ZrP Catalysts with Adjustable Ratio of Bronsted and Lewis Acids for the One-Pot Value-Added Conversion of Biomass-Derived Furfural. *ACS Sustain. Chem. Eng.* **2020**, *8*, 7403–7413. [[CrossRef](#)]
17. Maderuelo-Solera, R.; Richter, S.; Jiménez-Gómez, C.P.; García-Sancho, C.; García-Mateos, F.J.; Rosas, J.M.; Moreno-Tost, R.; Cecilia, J.A.; Maireles-Torres, P. Porous SiO₂ Nanospheres Modified with ZrO₂ and Their Use in One-Pot Catalytic Processes to Obtain Value-Added Chemicals from Furfural. *Ind. Eng. Chem. Res.* **2021**, *60*, 18791–18805. [[CrossRef](#)] [[PubMed](#)]
18. He, J.; Li, H.; Xu, Y.F.; Yang, S. Dual acidic mesoporous KIT silicates enable one-pot production of γ -valerolactone from biomass derivatives via cascade reactions. *Renew. Energy* **2020**, *146*, 359–370. [[CrossRef](#)]
19. Allegri, A.; Saotta, A.; Liuzzi, F.; Gianotti, E.; Paul, G.; Cattaneo, A.S.; Oldani, C.; Brigliadori, A.; Zanoni, I.; Fornasari, G.; et al. Aquivion-Based Spray Freeze-Dried Composite Materials for the Cascade Production of γ -Valerolactone. *ChemSusChem* **2024**, *17*, e202301683. [[CrossRef](#)]
20. Li, C.; Xu, G.Y.; Wang, C.G.; Ma, L.L.; Qiao, Y.; Zhang, Y.; Fu, Y. One-pot chemocatalytic transformation of cellulose to ethanol over Ru-WO_x/HZSM-5. *Green Chem.* **2019**, *21*, 2234–2239. [[CrossRef](#)]
21. Shi, X.Y.; Yang, Y.; Ye, X.; Zhong, H.; Wang, C.L.; Jin, F.M. Enhancing the Synergistic Effect of Bifunctional Pd-Based Catalyst by Phosphonic Acid for Cellobiose Conversion to Sorbitol. *ACS Sustain. Chem. Eng.* **2024**, *12*, 5991–6002. [[CrossRef](#)]
22. Gabriel, C.B.; Canhaci, S.J.; Borges, L.E.P.; Fraga, M.A. Aviation biofuel range cycloalkane from renewables: Liquid-phase catalytic conversion of menthol on niobia-supported catalysts. *Fuel* **2020**, *277*, 118288. [[CrossRef](#)]
23. Zhao, C.; He, J.Y.; Lemonidou, A.A.; Li, X.B.; Lercher, J.A. Aqueous-phase hydrodeoxygenation of bio-derived phenols to cycloalkanes. *J. Catal.* **2011**, *280*, 8–16. [[CrossRef](#)]
24. Zhang, J.X.; Bo, S.C.; Liao, W.P.; Yang, K.X.; Su, T.; Lue, H.Y.; Zhu, Z.G. Zeolitic framework Sn boosts the 2,5-dimethylfuran selectivity for the hydrodeoxygenation of 5-hydroxymethylfurfural over Co/Sn-Beta catalyst. *Chem. Eng. J.* **2024**, *484*, 149511. [[CrossRef](#)]
25. Tang, H.B.; Dai, Q.Q.; Cao, Y.; Wei, X.C.; Li, J.; Zou, X. In Situ Hydrodeoxygenation of Phenol as a Model Compound for Pyrolysis Oil Using Raney Ni and Molecular Sieve Catalysts. *Energy Fuels* **2021**, *35*, 4138–4147. [[CrossRef](#)]
26. Dijkmans, J.; Schutyser, W.; Dusselier, M.; Sels, B.F. Sn β -zeolite catalyzed oxido-reduction cascade chemistry with biomass-derived molecules. *Chem. Commun.* **2016**, *52*, 6712–6715. [[CrossRef](#)] [[PubMed](#)]
27. Liu, Y.C.; Zhou, S.W.; Wang, X.Y.; Qin, J.Y.; Hu, C.W.; Li, J.M. Coproduction of Glyceric Acid and Glycolic Acid from Biomass-Based Sugars over a Ru/Co₃O₄ Catalyst. *ACS Catal.* **2024**, *14*, 7609–7623. [[CrossRef](#)]
28. Jin, X.; Zhao, M.; Vora, M.; Shen, J.; Zeng, C.; Yan, W.J.; Thapa, P.S.; Subramaniam, B.; Chaudhari, R.V. Synergistic Effects of Bimetallic PtPd/TiO₂ Nanocatalysts in Oxidation of Glucose to Glucaric Acid: Structure Dependent Activity and Selectivity. *Ind. Eng. Chem. Res.* **2016**, *55*, 2932–2945. [[CrossRef](#)]
29. Zheng, Z.X.; Luo, Z.C.; Zhao, C. Morphologically Cross-Shaped Ru/HZSM-5 Catalyzes Tandem Hydrogenolysis of Guaiacol to Benzene in Water. *ChemCatChem* **2018**, *10*, 1376–1384. [[CrossRef](#)]
30. Yang, Y.; Ren, D.C.; Shang, C.L.; Ding, Z.Z.; Luo, X.R. Site isolated Ru clusters and sulfoacids in a yolk-shell nanoreactor towards cellulose valorization to 1,2-propylene glycol. *Chem. Eng. J.* **2023**, *452*, 139206. [[CrossRef](#)]
31. Rubulotta, G.; Luska, K.L.; Urbina-Blanco, C.A.; Eifert, T.; Palkovits, R.; Quadrelli, E.A.; Thieuleux, C.; Leitner, W. Highly Selective Hydrogenation of R-(+)-Limonene to (+)p-1-Menthene in Batch and Continuous Flow Reactors. *ACS Sustain. Chem. Eng.* **2017**, *5*, 3762–3767. [[CrossRef](#)]
32. Kulkarni, B.B.; Kanakikodi, K.S.; Maradur, S.P. Synergistic catalytic activity of core-shell Pd@UiO-66(Hf) MOF catalyst for the one-pot hydrogenation-esterification of furfural. *Microporous Mesoporous Mater.* **2022**, *343*, 112147. [[CrossRef](#)]
33. Li, S.; Liu, X.; Guo, Y.; Wang, Y. Room temperature synthesis of N-substituted pyrrolidone from levulinic acid and nitrobenzene via a tandem hydrogenation and reductive amination process. *J. Catal.* **2024**, *429*, 115191. [[CrossRef](#)]
34. Dapsens, P.Y.; Mondelli, C.; Pérez-Ramírez, J. Design of Lewis-acid centres in zeolitic matrices for the conversion of renewables. *Chem. Soc. Rev.* **2015**, *44*, 7025–7043. [[CrossRef](#)] [[PubMed](#)]
35. Ennaert, T.; Van Aelst, J.; Dijkmans, J.; De Clercq, R.; Schutyser, W.; Dusselier, M.; Verboekend, D.; Sels, B.F. Potential and challenges of zeolite chemistry in the catalytic conversion of biomass. *Chem. Soc. Rev.* **2016**, *45*, 584–611. [[CrossRef](#)]
36. Li, Y.; Li, L.; Yu, J.H. Applications of Zeolites in Sustainable Chemistry. *Chem* **2017**, *3*, 928–949. [[CrossRef](#)]
37. Sudarsanam, P.; Peeters, E.; Makshina, E.V.; Parvulescu, V.I.; Sels, B.F. Advances in porous and nanoscale catalysts for viable biomass conversion. *Chem. Soc. Rev.* **2019**, *48*, 2366–2421. [[CrossRef](#)] [[PubMed](#)]
38. Chai, Y.; Shang, W.; Li, W.; Wu, G.; Dai, W.; Guan, N.; Li, L. Noble metal particles confined in zeolites: Synthesis, characterization, and applications. *Adv. Sci.* **2019**, *6*, 1900299. [[CrossRef](#)]
39. Farrusseng, D.; Tuel, A. Perspectives on zeolite-encapsulated metal nanoparticles and their applications in catalysis. *New J. Chem.* **2016**, *40*, 3933–3949. [[CrossRef](#)]
40. Gao, C.; Lyu, F.; Yin, Y. Encapsulated Metal Nanoparticles for Catalysis. *Chem. Rev.* **2021**, *121*, 834–881. [[CrossRef](#)] [[PubMed](#)]

41. Mortensen, R.L.; Noack, H.-D.; Pedersen, K.; Mossin, S.; Mielby, J. Recent Advances in Complete Methane Oxidation using Zeolite-Supported Metal Nanoparticle Catalysts. *ChemCatChem* **2022**, *14*, e202101924. [[CrossRef](#)]
42. Xu, D.; Lv, H.; Liu, B. Encapsulation of metal nanoparticle catalysts within mesoporous zeolites and their enhanced catalytic performances: A review. *Front. Chem.* **2018**, *6*, 550. [[CrossRef](#)] [[PubMed](#)]
43. Zhai, Y.; Wang, K.; Sun, M.; Wang, F.; Zhang, X.; Lv, G.; Jiang, L.; Xu, Z. Manipulation of chemical behavior of species by a temperature-program strategy: Efficiently confining metal oxide nanoclusters in a hollow zeolite. *J. Mater. Chem. A* **2023**, *11*, 5775–5788. [[CrossRef](#)]
44. Yang, D.; Liu, X.; Zhao, W.N.; Yan, Q.; Song, F.; Wang, T.C.; Dai, Y.H.; Wan, X.Y.; Zhou, C.M.; Yang, Y.H. A survey of recent progress on novel catalytic materials with precise crystalline structures for oxidation/hydrogenation of key biomass platform chemicals. *EcoMat* **2021**, *3*, e12159. [[CrossRef](#)]
45. Lei, Q.F.; Wang, C.; Dai, W.L.; Wu, G.J.; Guan, N.J.; Li, L.D. Multifunctional heteroatom zeolites: Construction and applications. *Front. Chem. Sci. Eng.* **2021**, *15*, 1462–1486. [[CrossRef](#)]
46. Li, X.Y.; Ma, S.; Li, H. Zeolite confinement-catalyzed cleavage of C-O/C-C bonds in biomass. *Green Chem.* **2022**, *24*, 7243–7280. [[CrossRef](#)]
47. Krol, M. Natural vs. Synthetic Zeolites. *Crystals* **2020**, *10*, 622. [[CrossRef](#)]
48. Sherman, J.D. Synthetic zeolites and other microporous oxide molecular sieves. *Proc. Natl. Acad. Sci. USA* **1999**, *96*, 3471–3478. [[CrossRef](#)] [[PubMed](#)]
49. Diaz, I.; Kokkoli, E.; Terasaki, O.; Tsapatsis, M. Surface Structure of Zeolite (MFI) Crystals. *Chem. Mater.* **2004**, *16*, 5226–5232. [[CrossRef](#)]
50. Shamzhy, M.; Gil, B.; Opanasenko, M.; Roth, W.J.; Cejka, J. MWW and MFI Frameworks as Model Layered Zeolites: Structures, Transformations, Properties, and Activity. *ACS Catal.* **2021**, *11*, 2366–2396. [[CrossRef](#)]
51. Li, X.Y.; Han, H.; Xu, W.Q.; Hwang, S.J.; Shi, Z.C.; Lu, P.; Bhan, A.; Tsapatsis, M. Acid Catalysis over Low-Silica Faujasite Zeolites. *J. Am. Chem. Soc.* **2022**, *144*, 9324–9329. [[CrossRef](#)] [[PubMed](#)]
52. Bok, T.O.; Andriako, E.P.; Knyazeva, E.E.; Ivanova, I.I. Engineering of zeolite BEA crystal size and morphology via seed-directed steam assisted conversion. *RSC Adv.* **2020**, *10*, 38505–38514. [[CrossRef](#)] [[PubMed](#)]
53. Chassaing, S.; Beneteau, V.; Pale, P. Green catalysts based on zeolites for heterocycle synthesis. *Curr. Opin. Green Sustain. Chem.* **2018**, *10*, 35–39. [[CrossRef](#)]
54. de Aguiar Pedott, V.; Moraes, G.H.; Soares, C.; Padoin, N.; Riella, H.G.; Jose de Andrade, C. Biosurfactants as structure directing agents of porous siliceous materials. *Microporous Mesoporous Mater.* **2022**, *345*, 112279. [[CrossRef](#)]
55. Schlumberger, C.; Thommes, M. Characterization of Hierarchically Ordered Porous Materials by Physisorption and Mercury Porosimetry—A Tutorial Review. *Adv. Mater. Interfaces* **2021**, *8*, 2002181. [[CrossRef](#)]
56. Singh, B.K.; Kim, Y.; Kwon, S.; Na, K. Synthesis of Mesoporous Zeolites and Their Opportunities in Heterogeneous Catalysis. *Catalysts* **2021**, *11*, 1541. [[CrossRef](#)]
57. Weissenberger, T.; Machoke, A.G.F.; Reiprich, B.; Schwieger, W. Preparation and Potential Catalytic Applications of Hierarchically Structured Zeolites with Macropores. *Adv. Mater. Interfaces* **2021**, *8*, 2001653. [[CrossRef](#)]
58. Medeiros-Costa, I.C.; Laroche, C.; Perez-Pellitero, J.; Coasne, B. Characterization of hierarchical zeolites: Combining adsorption/intrusion, electron microscopy, diffraction and spectroscopic techniques. *Microporous Mesoporous Mater.* **2019**, *287*, 167–176. [[CrossRef](#)]
59. Reiprich, B.; Weissenberger, T.; Schwieger, W.; Inayat, A. Layer-like FAU-type zeolites: A comparative view on different preparation routes. *Front. Chem. Sci. Eng.* **2020**, *14*, 127–142. [[CrossRef](#)]
60. Roth, W.J.; Gil, B.; Makowski, W.; Marszalek, B.; Eliasova, P. Layer like porous materials with hierarchical structure. *Chem. Soc. Rev.* **2016**, *45*, 3400–3438. [[CrossRef](#)] [[PubMed](#)]
61. Tan, C.X.; He, C.J.; Sun, Y.Y.; Dong, H.; Ge, M.; Xia, X.P. A layer-like FAU zeolite with palladium particles embedded in situ as catalyst for hydrogenation of 1,4-bis(phenylethynyl) benzene. *Surf. Interfaces* **2022**, *34*, 102399. [[CrossRef](#)]
62. Nachtigall, P.; Delgado, M.R.; Nachtigallova, D.; Arean, C.O. The nature of cationic adsorption sites in alkaline zeolites—Single, dual and multiple cation sites. *Phys. Chem. Chem. Phys.* **2012**, *14*, 1552–1569. [[CrossRef](#)]
63. Yamamoto, K.; Ikeda, T. Prospects for a new zeolite synthesis route through alkaline-earth metal-containing microporous silicates. *Shokubai* **2018**, *60*, 266–272.
64. Ciantar, M.; Trinh, T.T.; Michel, C.; Sautet, P.; Mellot-Draznieks, C.; Nieto-Draghi, C. Impact of Organic Templates on the Selective Formation of Zeolite Oligomers. *Angew. Chem. -Int. Ed.* **2021**, *60*, 7111–7116. [[CrossRef](#)] [[PubMed](#)]
65. Lei, C.; Dong, Z.Y.; Martínez, C.; Martínez-Triguero, J.; Chen, W.; Wu, Q.M.; Meng, X.J.; Parvulescu, A.N.; De Baerdemaeker, T.; Müller, U.; et al. A Cationic Oligomer as an Organic Template for Direct Synthesis of Aluminosilicate ITH Zeolite. *Angew. Chem. -Int. Ed.* **2020**, *59*, 15649–15655. [[CrossRef](#)]
66. Asselman, K.; Pellens, N.; Thijs, B.; Doppelhammer, N.; Haouas, M.; Taulelle, F.; Martens, J.A.; Breynaert, E.; Kirschhock, C.E.A. Ion-Pairs in Aluminosilicate-Alkali Synthesis Liquids Determine the Aluminum Content and Topology of Crystallizing Zeolites. *Chem. Mater.* **2022**, *34*, 7150–7158. [[CrossRef](#)] [[PubMed](#)]
67. Li, J.L.; Gao, M.K.; Yan, W.F.; Yu, J.H. Regulation of the Si/Al ratios and Al distributions of zeolites and their impact on properties. *Chem. Sci.* **2023**, *14*, 1935–1959. [[CrossRef](#)] [[PubMed](#)]

68. Li, H.; Saravanamurugan, S.; Yang, S.; Riisager, A. Direct transformation of carbohydrates to the biofuel 5-ethoxymethylfurfural by solid acid catalysts. *Green Chem.* **2016**, *18*, 726–734. [[CrossRef](#)]
69. Zhu, D.L.; Wang, L.Y.; Fan, D.; Yan, N.N.; Huang, S.J.; Xu, S.T.; Guo, P.; Yang, M.; Zhang, J.M.; Tian, P.; et al. A Bottom-Up Strategy for the Synthesis of Highly Siliceous Faujasite-Type Zeolite. *Adv. Mater.* **2020**, *32*, 2000272. [[CrossRef](#)]
70. Moura, P.A.S.; Rodríguez-Aguado, E.; Maia, D.A.S.; Melo, D.C.; Singh, R.; Valencia, S.; Webley, P.A.; Rey, F.; Bastos-Neto, M.; Rodríguez-Castellón, E.; et al. Water adsorption and hydrothermal stability of CHA zeolites with different Si/Al ratios and compensating cations. *Catal. Today* **2022**, *390*, 99–108. [[CrossRef](#)]
71. Chen, B.F.; Xie, Z.B.; Peng, F.F.; Li, S.P.; Yang, J.N.; Wu, T.N.; Fan, H.L.; Zhang, Z.F.; Hou, M.Q.; Li, S.M.; et al. Production of Piperidine and δ -Lactam Chemicals from Biomass-Derived Triacetic Acid Lactone. *Angew. Chem. -Int. Ed.* **2021**, *60*, 14405–14409. [[CrossRef](#)] [[PubMed](#)]
72. Dijkmans, J.; Dusselier, M.; Gabriëls, D.; Houthoofd, K.; Magusin, P.; Huang, S.G.; Pontikes, Y.; Trekels, M.; Vantomme, A.; Giebel, L.; et al. Cooperative Catalysis for Multistep Biomass Conversion with Sn/Al Beta Zeolite. *ACS Catal.* **2015**, *5*, 928–940. [[CrossRef](#)]
73. An, H.; Kweon, S.; Kang, D.-C.; Shin, C.-H.; Kim, J.F.; Park, M.B.; Min, H.-K. Cascade conversion of glucose to 5-hydroxymethylfurfural over Bronsted-Lewis bi-acidic SnAl-beta zeolites. *Korean J. Chem. Eng.* **2021**, *38*, 1161–1169. [[CrossRef](#)]
74. Li, H.Q.; Pang, J.F.; Hu, W.D.; Caballero, V.; Sun, J.M.; Tan, M.W.; Hu, J.Z.; Ni, Y.L.; Wang, Y. Confined dual Lewis acid centers for selective cascade C-C coupling and deoxygenation. *Chem. Sci.* **2024**, *15*, 8031–8037. [[CrossRef](#)]
75. Jiang, J.; Ding, W.; Li, H. Promotional effect of F for Pd/HZSM-5 catalyst on selective HDO of biobased ketones. *Renew. Energy* **2021**, *179*, 1262–1270. [[CrossRef](#)]
76. Zhang, B.; Douthwaite, M.; Liu, Q.; Zhang, C.; Wu, Q.; Shi, R.; Wu, P.; Liu, K.; Wang, Z.; Lin, W.; et al. Seed- and solvent-free synthesis of ZSM-5 with tuneable Si/Al ratios for biomass hydrogenation. *Green Chem.* **2020**, *22*, 1630–1638. [[CrossRef](#)]
77. Zhao, R.R.; Li, S.K.; Bi, L.X.; Fu, Q.; Tan, H.Z.; Wang, M.; Cui, H.Y. Enhancement of *p*-xylene selectivity in the reaction between 2,5-dimethylfuran and ethanol over an ammonium fluoride-modified ZSM-5 zeolite. *Catal. Sci. Technol.* **2022**, *12*, 2248–2256. [[CrossRef](#)]
78. Yan, P.H.; Bryant, G.; Li, M.M.J.; Mensah, J.; Kennedy, E.; Stockenhuber, M. Shape selectivity of zeolite catalysts for the hydrodeoxygenation of biocrude oil and its model compounds. *Microporous Mesoporous Mater.* **2020**, *309*, 110561. [[CrossRef](#)]
79. Cnudde, P.; Demuynck, R.; Vandenbrande, S.; Waroquier, M.; Sastre, G.; Van Speybroeck, V. Light Olefin Diffusion during the MTO Process on H-SAPO-34: A Complex Interplay of Molecular Factors. *J. Am. Chem. Soc.* **2020**, *142*, 6007–6017. [[CrossRef](#)]
80. Yu, L.; Farinmade, A.; Ajumobi, O.; John, V.T.; Valla, J.A. One-Step Hydrothermal Tandem Reactions of *Miscanthus x giganteus* Using Ni Impregnated ZSM-5/MCM-41 Composites. *Energy Fuels* **2021**, *35*, 20117–20130. [[CrossRef](#)]
81. Zhang, J.J.; Zhao, C. Development of a Bimetallic Pd-Ni/HZSM-5 Catalyst for the Tandem Limonene Dehydrogenation and Fatty Acid Deoxygenation to Alkanes and Arenes for Use as Biojet Fuel. *ACS Catal.* **2016**, *6*, 4512–4525. [[CrossRef](#)]
82. Wang, H.W.; Lu, J.L. A Review on Particle Size Effect in Metal-Catalyzed Heterogeneous Reactions. *Chin. J. Chem.* **2020**, *38*, 1422–1444. [[CrossRef](#)]
83. Wang, P.S.; Yang, B.L.; Perumal, E.; Wu, Z.Q. Mechanism and kinetics of 1-phenyl-1,2-ethanediol cleavage catalyzed by Cu/Beta zeolite. *Int. J. Chem. Kinet.* **2022**, *54*, 391–399. [[CrossRef](#)]
84. Duong, N.; Tan, Q.H.; Resasco, D.E. Controlling phenolic hydrodeoxygenation by tailoring metal-O bond strength via specific catalyst metal type and particle size selection. *Comptes Rendus Chim.* **2018**, *21*, 155–163. [[CrossRef](#)]
85. Karanwal, N.; Sibi, M.G.; Khan, M.K.; Myint, A.A.; Ryu, B.C.; Kang, J.W.; Kim, J. Trimetallic Cu-Ni-Zn/H-ZSM-5 Catalyst for the One-Pot Conversion of Levulinic Acid to High-Yield 1,4-Pentanediol under Mild Conditions in an Aqueous Medium. *ACS Catal.* **2021**, *11*, 2846–2864. [[CrossRef](#)]
86. Zhao, M.; Wang, X.; Xu, J.; Li, Y.U.; Wang, X.M.; Chu, X.; Wang, K.; Wang, Z.J.; Zhang, L.L.; Feng, J.; et al. Strengthening the Metal-Acid Interactions by Using CeO₂ as Regulators of Precisely Placing Pt Species in ZSM-5 for Furfural Hydrogenation. *Adv. Mater.* **2024**, *36*, e202313596. [[CrossRef](#)] [[PubMed](#)]
87. Li, H.; Liu, H.M.; Cai, C.L.; Wang, H.Y.; Huang, Y.W.; Li, S.; Yang, B.; Wang, C.G.; Liao, Y.H.; Ma, L.L. Tandem conversion xylose to 2-methylfuran with NiCu/C catalyst. *Catal. Commun.* **2023**, *175*, 106625. [[CrossRef](#)]
88. Cho, H.J.; Kim, D.; Xu, B. Pore Size Engineering Enabled Selectivity Control in Tandem Catalytic Upgrading of Cyclopentanone on Zeolite-Encapsulated Pt Nanoparticles. *ACS Catal.* **2020**, *10*, 8850–8859. [[CrossRef](#)]
89. Barakov, R.; Shcherban, N.; Petrov, O.; Rainer, D.N.; Kubu, M.; Cejka, J.; Shamzhy, M.; Opanasenko, M. Optimization of Zr-Al-USY and Zr-Al-Beta zeolites catalysts for a one-pot cascade transformation of furfural to γ -valerolactone. *Catal. Today* **2024**, *426*, 114406. [[CrossRef](#)]
90. Gürbüz, E.I.; Gallo, J.M.R.; Alonso, D.M.; Wettstein, S.G.; Lim, W.Y.; Dumesic, J.A. Conversion of Hemicellulose into Furfural Using Solid Acid Catalysts in γ -Valerolactone. *Angew. Chem. -Int. Ed.* **2013**, *52*, 1270–1274. [[CrossRef](#)]
91. Verma, D.; Insyani, R.; Suh, Y.W.; Kim, S.M.; Kim, S.K.; Kim, J. Direct conversion of cellulose to high-yield methyl lactate over Ga-doped Zn/H-nanozeolite Y catalysts in supercritical methanol. *Green Chem.* **2017**, *19*, 1969–1982. [[CrossRef](#)]
92. Song, S.; Di, L.; Wu, G.J.; Dai, W.L.; Guan, N.J.; Li, L.D. Meso-Zr-Al-beta zeolite as a robust catalyst for cascade reactions in biomass valorization. *Appl. Catal. B-Environ.* **2017**, *205*, 393–403. [[CrossRef](#)]

93. Osatiashtiani, A.; Puértolas, B.; Oliveira, C.C.S.; Manayil, J.C.; Barbero, B.; Isaacs, M.; Michailof, C.; Heracleous, E.; Pérez-Ramírez, J.; Lee, A.F.; et al. On the influence of Si:Al ratio and hierarchical porosity of FAU zeolites in solid acid catalysed esterification pretreatment of bio-oil. *Biomass Convers. Biorefin.* **2017**, *7*, 331–342. [[CrossRef](#)]
94. Tang, H.B.; Dai, Q.Q.; Cao, Y.; Wei, X.C.; Jibrán, K.; Li, J. Hydrodeoxygenation of phenol and pyrolysis oil using Raney Ni and IL/Zr-SBA-15 catalysts. *J. Environ. Chem. Eng.* **2021**, *9*, 105848. [[CrossRef](#)]
95. Santos, R.C.R.; Braga, D.M.V.; Pinheiro, A.N.; Leite, E.R.; Freire, V.N.; Longhinotti, E.; Valentini, A. Role of Cu, Ni and Co metals in the acidic and redox properties of Mo catalysts supported on Al₂O₃ spheres for glycerol conversion. *Catal. Sci. Technol.* **2016**, *6*, 4986–5002. [[CrossRef](#)]
96. Altug, C.; Munoz-Batista, M.J.; Rodriguez-Padron, D.; Balu, A.M.; Romero, A.A.; Luque, R. Continuous flow synthesis of amines from the cascade reactions of nitriles and carbonyl-containing compounds promoted by Pt-modified titania catalysts. *Green Chem.* **2019**, *21*, 300–306. [[CrossRef](#)]
97. Li, W.; Xu, S.G.; Xu, X. Valorisation of Corncob Residue towards the Sustainable Production of Glucuronic Acid. *Catalysts* **2022**, *12*, 1603. [[CrossRef](#)]
98. Wang, Y.Z.; De, S.; Yan, N. Rational control of nano-scale metal-catalysts for biomass conversion. *Chem. Commun.* **2016**, *52*, 6210–6224. [[CrossRef](#)] [[PubMed](#)]
99. Godino-Ojer, M.; Blazquez-García, R.; Matos, I.; Bernardo, M.; Fonseca, I.M.; Mayoral, E.P. Porous carbons-derived from vegetal biomass in the synthesis of quinoxalines. Mechanistic insights. *Catal. Today* **2020**, *354*, 90–99. [[CrossRef](#)]
100. Wu, Q.; Zhang, G.Y.; Gao, M.M.; Cao, S.S.; Li, L.; Liu, S.W.; Xie, C.X.; Huang, L.; Yu, S.T.; Ragauskas, A.J. Clean production of 5-hydroxymethylfurfural from cellulose using a hydrothermal/biomass-based carbon catalyst. *J. Clean. Prod.* **2019**, *213*, 1096–1102. [[CrossRef](#)]
101. An, H.; Kim, Y.W.; Kweon, S.; Son, Y.M.; Kim, J.F.; Shin, C.H.; Kang, S.B.; Park, M.B.; Min, H.K. Cascade conversion of glucose to 5-hydroxymethylfurfural over Bronsted-Lewis bi-acidic SiO₂-ZrO₂ catalysts. *Biomass Convers. Biorefin.* **2023**, *13*, 11779–11787. [[CrossRef](#)]
102. Saravanan, K.; Park, K.S.; Jeon, S.; Bae, J.W. Aqueous Phase Synthesis of 5-Hydroxymethylfurfural from Glucose over Large Pore Mesoporous Zirconium Phosphates: Effect of Calcination Temperature. *ACS Omega* **2018**, *3*, 808–820. [[CrossRef](#)] [[PubMed](#)]
103. Shinde, S.; Rode, C. Cascade Reductive Etherification of Bioderived Aldehydes over Zr-Based Catalysts. *ChemSusChem* **2017**, *10*, 4090–4101. [[CrossRef](#)] [[PubMed](#)]
104. Wang, J.A.; Liu, Y.F.; Wang, J.H.; Liu, T.H.; Pang, Z.B.; Cui, H.Y.; Zhang, Y.; Song, F. Cooperative catalysis of carbon supported zinc salts hybrid for efficient conversion of fructose to ethyl lactate. *Chem. Eng. J.* **2023**, *468*, 143670. [[CrossRef](#)]
105. Antunes, M.M.; Lima, S.; Fernandes, A.; Ribeiro, M.F.; Chadwick, D.; Hellgardt, K.; Pillinger, M.; Valente, A.A. One-pot hydrogen production and cascade reaction of furfural to bioproducts over bimetallic Pd-Ni TUD-1 type mesoporous catalysts. *Appl. Catal. B-Environ.* **2018**, *237*, 521–537. [[CrossRef](#)]
106. Wu, C.M.; Li, J.F.; Liu, C.L.; Dong, W.S. Insight into the enhanced catalytic performance of phosphate-modified ZrO₂/SBA-15 for the conversion of biobased 2,5-dimethylfuran and ethylene into *p*-xylene. *Chem. Eng. J.* **2024**, *480*, 148031. [[CrossRef](#)]
107. Zhang, X.Y.; Li, Y.; Xue, L.F.; Wang, S.T.; Wang, X.H.; Jiang, Z.J. Catalyzing Cascade Production of Methyl Levulinate from Polysaccharides Using Heteropolyacids H_nPW₁₁MO₃₉ with Bronsted/Lewis Acidic Sites. *ACS Sustain. Chem. Eng.* **2018**, *6*, 165–176. [[CrossRef](#)]
108. Cui, Y.N.; Zhang, Y.L.; Yu, F.; Fu, S.Q.; Yao, Q.X.; Chen, Y.L.; Zhang, M.Y.; Huang, X.Q.; Shen, G.D.; Sun, D. In-situ self-assembly of two ultrastable bifunctional Keggin-type polyoxometalates-based zeolite-like frameworks for efficient cascade biomass chemicals conversion. *J. Catal.* **2024**, *429*, 115268. [[CrossRef](#)]
109. Zhang, X.Y.; Zhang, D.; Sun, Z.; Xue, L.F.; Wang, X.H.; Jiang, Z.J. Highly efficient preparation of HMF from cellulose using temperature-responsive heteropolyacid catalysts in cascade reaction. *Appl. Catal. B-Environ.* **2016**, *196*, 50–56. [[CrossRef](#)]
110. Zhang, J.; Chen, J.Z. Selective Transfer Hydrogenation of Biomass-Based Furfural and 5-Hydroxymethylfurfural over Hydrotalcite-Derived Copper Catalysts Using Methanol as a Hydrogen Donor. *ACS Sustain. Chem. Eng.* **2017**, *5*, 5982–5993. [[CrossRef](#)]
111. Deng, T.Y.; Xu, G.Y.; Fu, Y. One-pot cascade conversion of xylose to furfuryl alcohol over a bifunctional Cu/SBA-15-SO₃H catalyst. *Chin. J. Catal.* **2020**, *41*, 404–414. [[CrossRef](#)]
112. Chary, K.V.R.; Srikanth, C.S.; Rao, V.V. Characterization and reactivity of Nb₂O₅ supported Ru catalysts. *Catal. Commun.* **2009**, *10*, 459–463. [[CrossRef](#)]
113. Aranda, D.A.G.; Ramos, A.L.D.; Passos, F.B.; Schmal, M. Characterization and dehydrogenation activity of Pt/Nb₂O₅ catalysts. *Catal. Today* **1996**, *28*, 119–125. [[CrossRef](#)]
114. Xu, Y.; Nie, G.K.; Jiang, X.; Wang, H.Y.; Yang, G.H.; Yan, Z.Y.; Zou, J.J.; Yu, H.L.; Yu, S.T.; Liu, Y. Synthesis of 1-hexanol by highly selective hydrodeoxygenation of 5-hydroxymethylfurfural using Ni/MCM-41 and Pt-WO_x/t-ZrO₂. *Chem. Eng. J.* **2024**, *487*, 150695. [[CrossRef](#)]
115. Li, J.M.; Yang, R.F.; Xu, S.G.; Zhou, C.Q.; Xiao, Y.; Hu, C.W.; Tsang, D.C.W. Biomass-derived polyols valorization towards glycolic acid production with high atom-economy. *Appl. Catal. B-Environ.* **2022**, *317*, 121785. [[CrossRef](#)]
116. Gao, Z.X.; Zhao, X.X.; Li, X.M.; Wu, H.F.; Gao, M.Y.; Wang, Q.; Li, D.Q.; Feng, J.T. Rational regulation of spatially adjacent Al₄c and Al₆c sites assisted Ru catalysts for low-NH₃ furfural tandem reductive amination. *Chem. Eng. Sci.* **2022**, *258*, 117777. [[CrossRef](#)]

117. Wang, L.; Yang, Y.; Shi, Y.; Liu, W.; Tian, Z.; Zhang, X.; Zheng, L.; Hong, S.; Wei, M. Single-atom catalysts with metal-acid synergistic effect toward hydrodeoxygenation tandem reactions. *Chem Catal.* **2023**, *3*, 100483. [[CrossRef](#)]
118. Wang, J.A.; Wang, J.H.; Liu, Y.F.; Liu, T.H.; Pang, Z.B.; Cui, H.Y.; Zhang, Y.; Song, F. Temperature-responsive Zn-based catalysts for efficient catalytic conversion of biomass-derived carbohydrates to ethyl lactate. *Green Chem.* **2023**, *25*, 5613–5625. [[CrossRef](#)]
119. Liu, Y.T.; Wu, Y.Q.; He, Y.C.; Ma, C.L. Synthesis of furoic acid from biomasses by sequential catalysis with fish scale-rice husk-based heterogeneous chemocatalyst and dehydrogenase biocatalyst. *Ind. Crops Prod.* **2023**, *202*, 117033. [[CrossRef](#)]
120. Kumar, A.; Bal, R.; Srivastava, R. Pd-Decorated CePO₄ Catalyst for the One-Pot, Two-Step Cascade Reaction to Transform Biomass-Derived Furanic Aldehydes into Fuel Intermediates. *Energy Fuels* **2021**, *35*, 11366–11381. [[CrossRef](#)]
121. Yuan, K.; Zhao, W.; Zhou, Y.; Zhang, X.; Chen, S.; Chen, J.; Liu, C.; Xiong, W. Strategies for Selective Synthesis of Biomass-Based 1,13-Tridecanediol from Furfural. *ACS Sustainable Chem. Eng.* **2023**, *11*, 17769–17777. [[CrossRef](#)]
122. Rodiansono; Astuti, M.D.; Mustikasari, K.; Husain, S.; Sutomo. Recent progress in the direct synthesis of γ -valerolactone from biomass-derived sugars catalyzed by RANEY[®] Ni-Sn alloy supported on aluminium hydroxide. *Catal. Sci. Technol.* **2020**, *10*, 7768–7778. [[CrossRef](#)]
123. Fang, Q.H.; Qin, Z.X.; Shi, Y.Y.; Liu, F.; Barkaoui, S.; Abroshan, H.; Li, G. Au/NiO Composite: A Catalyst for One-Pot Cascade Conversion of Furfural. *ACS Appl. Energy Mater.* **2019**, *2*, 2654–2661. [[CrossRef](#)]
124. Zhao, J.; Yan, Y.B.; Hu, Z.T.; Jose, S.; Chen, X.P.; Lee, J.M. Bifunctional carbon nanoplatelets as metal-free catalysts for direct conversion of fructose to 2,5-diformylfuran. *Catal. Sci. Technol.* **2020**, *10*, 4179–4183. [[CrossRef](#)]
125. Yu, Z.H.; Ji, N.; Xiong, J.; Han, Y.; Li, X.Y.; Zhang, R.; Qiao, Y.N.; Zhang, M.; Lu, X.B. Ultrafine Ruthenium Clusters Shell-Embedded Hollow Carbon Spheres as Nanoreactors for Channel Microenvironment-Modulated Furfural Tandem Hydrogenation. *Small* **2022**, *18*, e2201361. [[CrossRef](#)]
126. Wang, L.; Wu, Y.C.; Zhang, H.J.; Li, H.; Liang, Y.X.; Long, B.X.; Wang, X.C. One-pot catalytic conversion of sugars to methyl lactate over acid-base bifunctional Sn/MgO catalysts. *Catal. Today* **2024**, *434*, 114701. [[CrossRef](#)]
127. Hou, W.; Wang, Q.; Guo, Z.J.; Li, J.; Zhou, Y.; Wang, J. Nanobelt α -CuV₂O₆ with hydrophilic mesoporous poly(ionic liquid): A binary catalyst for synthesis of 2,5-diformylfuran from fructose. *Catal. Sci. Technol.* **2017**, *7*, 1006–1016. [[CrossRef](#)]
128. Eblagon, K.M.; Pereira, M.F.R.; Figueiredo, J.L. One-pot oxidation of cellobiose to gluconic acid. Unprecedented high selectivity on bifunctional gold catalysts over mesoporous carbon by integrated texture and surface chemistry optimization. *Appl. Catal. B-Environ.* **2016**, *184*, 381–396. [[CrossRef](#)]
129. Zhou, C.M.; Deng, W.P.; Wan, X.Y.; Zhang, Q.H.; Yang, Y.H.; Wang, Y. Functionalized Carbon Nanotubes for Biomass Conversion: The Base-Free Aerobic Oxidation of 5-Hydroxymethylfurfural to 2,5-Furandicarboxylic Acid over Platinum Supported on a Carbon Nanotube Catalyst. *Chemcatchem* **2015**, *7*, 2853–2863. [[CrossRef](#)]
130. Li, Z.; Tian, K.; Wang, K.; Li, Z.; Qin, H.; Li, H. Acidic Magnetic Biocarbon-Enabled Upgrading of Biomass-Based Hexanedione into Pyrroles. *J. Renew. Mater.* **2023**, *11*, 3847–3865. [[CrossRef](#)]
131. Wang, K.P.; Wu, M.; Liu, Y.X.; Yang, Y.; Li, H. Magnetic solid sulfonic acid-enabled direct catalytic production of biomass-derived *N*-substituted pyrroles. *New J. Chem.* **2022**, *46*, 5312–5320. [[CrossRef](#)]
132. Li, Q.; Ma, C.L.; Zhang, P.Q.; Li, Y.Y.; Zhu, X.; He, Y.C. Effective conversion of sugarcane bagasse to furfural by coconut shell activated carbon-based solid acid for enhancing whole-cell biosynthesis of furfurylamine. *Ind. Crops Prod.* **2021**, *160*, 113169. [[CrossRef](#)]
133. García, A.; Saotta, A.; Miguel, P.J.; Sánchez-Tovar, R.; Fornasari, G.; Allegri, A.; Torres-Olea, B.; Cecilia, J.A.; Albonetti, S.; Dimitratos, N.; et al. Promoter Effect of Pt on Zr Catalysts to Increase the Conversion of Furfural to γ -Valerolactone Using Batch and Continuous Flow Reactors: Influence of the Way of the Incorporation of the Pt Sites. *Energy Fuels* **2024**, *38*, 9849–9861. [[CrossRef](#)] [[PubMed](#)]
134. Yaghi, O.M.; Li, H. Hydrothermal Synthesis of a Metal-Organic Framework Containing Large Rectangular Channels. *J. Am. Chem. Soc.* **1995**, *117*, 10401. [[CrossRef](#)]
135. Gong, W.; Liu, Y.; Li, H.; Cui, Y. Metal-organic frameworks as solid Bronsted acid catalysts for advanced organic transformations. *Coord. Chem. Rev.* **2020**, *420*, 213400. [[CrossRef](#)]
136. Gangu, K.K.; Jonnalagadda, S.B. A Review on Metal-Organic Frameworks as Congenial Heterogeneous Catalysts for Potential Organic Transformations. *Front. Chem.* **2021**, *9*, 747615. [[CrossRef](#)] [[PubMed](#)]
137. Qin, Y.T.; Guo, J.; Zhao, M.T. Metal-Organic Framework-Based Solid Acid Materials for Biomass Upgrade. *Trans. Tianjin Univ.* **2021**, *27*, 434–449. [[CrossRef](#)]
138. Zou, M.M.; Dong, M.; Zhao, T. Advances in Metal-Organic Frameworks MIL-101(Cr). *Int. J. Mol. Sci.* **2022**, *23*, 9396. [[CrossRef](#)] [[PubMed](#)]
139. Zhang, P.; Hou, P.; Ma, M.W.; Bu, K.; Guo, Q.; Yue, H.J.; Tian, G.; Feng, S.H. Bifunctional zirconium-based metal-organic frameworks as chemoselective catalysts for the synthesis of γ -valerolactone from furfural via a one-pot cascade reaction. *Appl. Catal. A Gen.* **2023**, *653*, 119064. [[CrossRef](#)]
140. Li, W.K.; Cai, Z.; Li, H.; Shen, Y.; Zhu, Y.Q.; Li, H.C.; Zhang, X.B.; Wang, F.M. Hf-based metal organic frameworks as bifunctional catalysts for the one-pot conversion of furfural to γ -valerolactone. *Mol. Catal.* **2019**, *472*, 17–26. [[CrossRef](#)]
141. Rahaman, M.S.; Tulaphol, S.; Hossain, M.A.; Jasinski, J.B.; Sun, N.; George, A.; Simmons, B.A.; Maihom, T.; Crocker, M.; Sathitsuksanoh, N. Cooperative Bronsted-Lewis acid sites created by phosphotungstic acid encapsulated metal-organic frameworks for selective glucose conversion to 5-hydroxymethylfurfural. *Fuel* **2022**, *310*, 122459. [[CrossRef](#)]

142. Li, J.; Zhao, S.H.; Li, Z.; Liu, D.; Chi, Y.N.; Hu, C.W. Efficient Conversion of Biomass-Derived Levulinic Acid to γ -Valerolactone over Polyoxometalate@Zr-Based Metal-Organic Frameworks: The Synergistic Effect of Bronsted and Lewis Acidic Sites. *Inorg. Chem.* **2021**, *60*, 7785–7793. [[CrossRef](#)] [[PubMed](#)]
143. Zeng, D.; Wang, W.J.; Zhang, Y.; Wang, J.X.; Cui, B.K.; Jia, T.K.; Li, R.F.; Chu, H.X.; Zhang, L.; Wang, W.Z. Efficient One-Pot Synthesis of 2,5-Furandicarboxylic Acid from Sugars over Polyoxometalate/Metal-Organic Framework Catalysts. *ChemSusChem* **2023**, *16*, e202300836. [[CrossRef](#)] [[PubMed](#)]
144. Zhang, X.B.; Chen, L.N.; Li, Y.J.; Li, H.Q.; Xie, Z.X.; Kuang, Q.; Zheng, L.S. Palladium NPs supported on sulfonic acid functionalized metal-organic frameworks as catalysts for biomass cascade reactions. *Dalton Trans.* **2019**, *48*, 5515–5519. [[CrossRef](#)] [[PubMed](#)]
145. Yang, J.; Huang, W.J.; Liu, Y.S.; Zhou, T. Enhancing the conversion of ethyl levulinate to γ -valerolactone over Ru/UiO-66 by introducing sulfonic groups into the framework. *RSC Adv.* **2018**, *8*, 16611–16618. [[CrossRef](#)]
146. Wei, Y.N.; Zhang, Y.L.; Li, B.; Guan, W.; Yan, C.H.; Li, X.; Yan, Y.S. Facile synthesis of metal-organic frameworks embedded in interconnected macroporous polymer as a dual acid-base bifunctional catalyst for efficient conversion of cellulose to 5-hydroxymethylfurfural. *Chin. J. Chem. Eng.* **2022**, *44*, 169–181. [[CrossRef](#)]
147. Zhang, H.; Cheng, F.; Li, Y.; He, C.; Li, H.; Yang, S. Polymeric organophosphate-hafnium unconventional MOFs nanohybrids enable high-efficiency upgrading of biomass feedstocks via cascade catalytic transfer hydrogenation-dehydration. *Ind. Crops Prod.* **2022**, *188*, 115606. [[CrossRef](#)]
148. Rani, P.; Srivastava, R. Multi-functional metal-organic framework and metal-organic framework-zeolite nanocomposite for the synthesis of carbohydrate derived chemicals via one-pot cascade reaction. *J. Colloid Interface Sci.* **2019**, *557*, 144–155. [[CrossRef](#)] [[PubMed](#)]
149. Cai, Z.Q.; Zhang, Z.Y.; Qi, Y.X.; Zheng, C.L.; Wei, X.S.; Cheng, Z.F.; Feng, Y.S. Selective conversion of furfural to cyclopentanone over the N-doped CuNi alloy carbon materials derived from porphyrin-based bimetallic metal-organic frameworks. *Fuel* **2024**, *371*, 131898. [[CrossRef](#)]
150. Yuan, L.Y.; Zhang, M.; Fan, G.L.; Li, F. Remarkably boosting ethanol upgrading to higher alcohols through cooperative catalysis of surface-interface multiple-active sites on nitrogen-doped carbon decorated copper-based catalysts. *Appl. Catal. B-Environ. Energy* **2024**, *343*, 123488. [[CrossRef](#)]
151. Park, J.; Mushtaq, U.; Sugiarto, J.R.; Verma, D.; Kim, J. Total chemocatalytic cascade conversion of lignocellulosic biomass into biochemicals. *Appl. Catal. B-Environ.* **2022**, *310*, 121280. [[CrossRef](#)]
152. Xia, Z.H.; Niu, L.B.; Wu, Q.; An, Y.D.; Bai, G.Y. Construction of isolated Co-N_x and dual Co_n-CoN_x sites for the regulation of hydrogenation and hydrodeoxygenation selectivity of biomass-derived chemicals. *Green Chem.* **2023**, *25*, 9313–9321. [[CrossRef](#)]
153. Li, X.; Zhang, L.K.; Zhou, R.; Chen, S.X.; Wang, J.; Zeng, Z.L.; Zou, J.J.; Deng, S.G.; Deng, Q. Bifunctional Role of Hydrogen in Aqueous Hydrogenative Ring Rearrangement of Furfurals over Co@Co-NC. *ACS Sustain. Chem. Eng.* **2022**, *10*, 7321–7329. [[CrossRef](#)]
154. Zorzetto, F.; Ballesteros-Plata, D.; Perosa, A.; Rodríguez-Castellón, E.; Selva, M.; Rodríguez-Padrón, D. Orthogonal assisted tandem reactions for the upgrading of bio-based aromatic alcohols using chitin derived mono and bimetallic catalysts. *Green Chem.* **2024**, *26*, 5221–5238. [[CrossRef](#)]
155. Wu, J.; Jin, M.; Li, Y.; Zhao, J.F.; Wang, T.T.; Xie, Y.H.; Liu, L.Q.; Wang, C.B.; Li, F.W. Earth-abundant Co nanoparticles encapsulated in N-doped hollow carbon sphere for highly selective hydrodeoxygenation of biomass-derived vanillin. *Chem. Eng. J.* **2023**, *463*, 142472. [[CrossRef](#)]
156. Parrilla-Lahoz, S.; Jin, W.; Pastor-Pérez, L.; Duyar, M.S.; Martínez-Quintana, L.; Dongil, A.B.; Reina, T.R. Multicomponent graphene based catalysts for guaiacol upgrading in hydrothermal conditions: Exploring “H₂-free” alternatives for bio-compounds hydrodeoxygenation. *Catal. Today* **2023**, *423*, 114020. [[CrossRef](#)]
157. Sulman, A.M.; Matveeva, V.G.; Bronstein, L.M. Cellulase immobilization on nanostructured supports for biomass waste processing. *Nanomaterials* **2022**, *12*, 3796. [[CrossRef](#)]
158. Sulman, E.M.; Matveeva, V.G.; Bronstein, L.M. Design of biocatalysts for efficient catalytic processes. *Curr. Opin. Chem. Eng.* **2019**, *26*, 1–8. [[CrossRef](#)]
159. Kourist, R.; Gonzalez-Sabin, J. Non-conventional media as strategy to overcome the solvent dilemma in chemoenzymatic tandem catalysis. *ChemCatChem* **2020**, *12*, 1903–1912. [[CrossRef](#)]
160. Monterrey, D.T.; Ayuso-Fernandez, I.; Oroz-Guinea, I.; Garcia-Junceda, E. Design and biocatalytic applications of genetically fused multifunctional enzymes. *Biotechnol. Adv.* **2022**, *60*, 108016. [[CrossRef](#)]
161. Reisenbauer, J.C.; Sicinski, K.M.; Arnold, F.H. Catalyzing the future: Recent advances in chemical synthesis using enzymes. *Curr. Opin. Chem. Biol.* **2024**, *83*, 102536. [[CrossRef](#)] [[PubMed](#)]
162. Zhang, Z.-G.; Jiang, S.-K.; Shen, X.; Lin, J.-C.; Yi, Y.; Ji, X.-J. Biocatalytic synthesis of vanillin from biomass-derived compounds: A review. *Catal. Today* **2025**, *445*, 115077. [[CrossRef](#)]
163. Kumar, V.; Patel, S.K.S.; Gupta, R.K.; Otari, S.V.; Gao, H.; Lee, J.-K.; Zhang, L. Enhanced Saccharification and Fermentation of Rice Straw by Reducing the Concentration of Phenolic Compounds Using an Immobilized Enzyme Cocktail. *Biotechnol. J.* **2019**, *14*, e1800468. [[CrossRef](#)]

164. Huang, Y.; Li, J.; Yang, Y.; Yuan, H.; Wei, Q.; Liu, X.; Zhao, Y.; Ni, C. Characterization of enzyme-immobilized catalytic support and its exploitation for the degradation of methoxychlor in simulated polluted soils. *Environ. Sci. Pollut. Res.* **2019**, *26*, 28328–28340. [[CrossRef](#)]
165. Chen, Q.; Liu, D.; Wu, C.; Yao, K.; Li, Z.; Shi, N.; Wen, F.; Gates, I.D. Co-immobilization of cellulase and lysozyme on amino-functionalized magnetic nanoparticles: An activity-tunable biocatalyst for extraction of lipids from microalgae. *Bioresour. Technol.* **2018**, *263*, 317–324. [[CrossRef](#)] [[PubMed](#)]
166. Yi, J.; Qiu, M.; Zhu, Z.; Dong, X.; Andrew Decker, E.; McClements, D.J. Robust and recyclable magnetic nanobiocatalysts for extraction of anthocyanin from black rice. *Food Chem.* **2021**, *364*, 130447. [[CrossRef](#)] [[PubMed](#)]
167. Paz-Cedeno, F.R.; Carceller, J.M.; Iborra, S.; Donato, R.K.; Godoy, A.P.; Veloso de Paula, A.; Monti, R.; Corma, A.; Masarin, F. Magnetic graphene oxide as a platform for the immobilization of cellulases and xylanases: Ultrastructural characterization and assessment of lignocellulosic biomass hydrolysis. *Renew. Energy* **2021**, *164*, 491–501. [[CrossRef](#)]
168. Amaro-Reyes, A.; Diaz-Hernandez, A.; Gracida, J.; Garcia-Almendarez, B.E.; Escamilla-Garcia, M.; Arredondo-Ochoa, T.; Regalado, C. Enhanced performance of immobilized xylanase/filter paper-ase on a magnetic chitosan support. *Catalysts* **2019**, *9*, 966. [[CrossRef](#)]
169. Paz-Cedeno, F.R.; Carceller, J.M.; Iborra, S.; Donato, R.K.; Rodriguez, A.F.R.; Morales, M.A.; Solorzano-Chavez, E.G.; Roldan, I.U.M.; de Paula, A.V.; Masarin, F. Stability of the Cellic CTec2 enzymatic preparation immobilized onto magnetic graphene oxide: Assessment of hydrolysis of pretreated sugarcane bagasse. *Ind. Crops Prod.* **2022**, *183*, 114972. [[CrossRef](#)]
170. Kirupa Sankar, M.; Ravikumar, R.; Naresh Kumar, M.; Sivakumar, U. Development of co-immobilized tri-enzyme biocatalytic system for one-pot pretreatment of four different perennial lignocellulosic biomass and evaluation of their bioethanol production potential. *Bioresour. Technol.* **2018**, *269*, 227–236. [[CrossRef](#)] [[PubMed](#)]
171. González-Granda, S.; Escot, L.; Lavandera, I.; Gotor-Fernández, V. Chemoenzymatic Cascades Combining Biocatalysis and Transition Metal Catalysis for Asymmetric Synthesis. *Angew. Chem. -Int. Ed.* **2023**, *62*, e202217713. [[CrossRef](#)] [[PubMed](#)]
172. Terholsen, H.; Meyer, J.R.H.; Zhang, Z.L.; Deuss, P.J.; Bornscheuer, U.T. Chemoenzymatic Cascade Reaction for the Valorization of the Lignin Depolymerization Product G-C2-Dioxolane Phenol. *ChemSusChem* **2023**, *16*, e202300168. [[CrossRef](#)] [[PubMed](#)]
173. He, W.; Ni, J.C.; He, Y.C.; Ye, J.R. Chemoenzymatic catalytic synthesis of furfurylamine from hemicellulose in biomasses. *Int. J. Biol. Macromol.* **2022**, *222*, 1201–1210. [[CrossRef](#)] [[PubMed](#)]
174. Liang, J.G.; Ji, L.; He, J.R.; Tang, S.X.; He, Y.C. Chemoenzymatic Conversion of Biomass-Derived D-Xylose to Furfuryl Alcohol with Corn Stalk-Based Solid Acid Catalyst and Reductase Biocatalyst in a Deep Eutectic Solvent-Water System. *Processes* **2022**, *10*, 113. [[CrossRef](#)]
175. Feng, X.Q.; Zhang, L.; Zhu, X.; Xia, Y.; Ma, C.L.; Liang, J.G.; He, Y.C. A Hybrid Catalytic Conversion of Corn cob to Furfurylamine in Tandem Reaction with Aluminium-Based Alkaline-Treated Graphite and ω -Transaminase Biocatalyst in γ -Valerolactone-Water. *Catal. Lett.* **2021**, *151*, 1834–1841. [[CrossRef](#)]
176. Li, Q.; Di, J.H.; Liao, X.L.; Ni, J.C.; Li, Q.; He, Y.C.; Ma, C.L. Exploration of benign deep eutectic solvent-water systems for the highly efficient production of furfurylamine from sugarcane bagasse via chemoenzymatic cascade catalysis. *Green Chem.* **2021**, *23*, 8154–8168. [[CrossRef](#)]
177. Li, Y.Y.; Li, Q.; Zhang, P.Q.; Ma, C.L.; Xu, J.H.; He, Y.C. Catalytic conversion of corn cob to furfuryl alcohol in tandem reaction with tin-loaded sulfonated zeolite and NADPH-dependent reductase biocatalyst. *Bioresour. Technol.* **2021**, *320*, 124267. [[CrossRef](#)]
178. Qin, L.Z.; He, Y.C. Chemoenzymatic Synthesis of Furfuryl Alcohol from Biomass in Tandem Reaction System. *Appl. Biochem. Biotechnol.* **2020**, *190*, 1289–1303. [[CrossRef](#)]
179. Feng, X.Q.; Li, Y.Y.; Ma, C.L.; Xia, Y.; He, Y.C. Improved conversion of bamboo shoot shells to furfuryl alcohol and furfurylamine by a sequential catalysis with sulfonated graphite and biocatalysts. *RSC Adv.* **2020**, *10*, 40365–40372. [[CrossRef](#)] [[PubMed](#)]
180. Di, J.H.; Zhang, L.; Tang, Z.Y.; Feng, X.Q.; He, Y.C. A Hybrid Strategy for the Efficient Biosynthesis of Fufuryl Alcohol from Corn cob in Formic Acid-Water. *Catal. Lett.* **2023**, *153*, 682–688. [[CrossRef](#)]
181. He, A.Y.; Dong, L.L.; Xu, N.; El-Hout, S.I.; Xia, J.; Qiu, Z.Y.; He, J.L.; Deng, Y.F.; Liu, X.Y.; Hu, L.; et al. Complete oxidation of 5-hydroxymethylfurfural to 2,5-furandicarboxylic acid by a novel enzyme-nanozyme hybrid catalyst. *Chem. Eng. J.* **2022**, *449*, 137797. [[CrossRef](#)]
182. Di, J.H.; Zhao, N.N.; Fan, B.; He, Y.C.; Ma, C.L. Efficient Valorization of Sugarcane Bagasse into Furfurylamine in Benign Deep Eutectic Solvent ChCl:Gly-Water. *Appl. Biochem. Biotechnol.* **2022**, *194*, 2204–2218. [[CrossRef](#)] [[PubMed](#)]
183. Arias, K.S.; Carceller, J.M.; Climent, M.J.; Corma, A.; Iborra, S. Chemoenzymatic Synthesis of 5-Hydroxymethylfurfural (HMF)-Derived Plasticizers by Coupling HMF Reduction with Enzymatic Esterification. *ChemSusChem* **2020**, *13*, 1864–1875. [[CrossRef](#)]
184. Wang, H.X.; Wang, Y.Q.; Huang, L.; Geng, A.Y.; Yi, F.J.; Zhu, Y.L.; Li, Y.W. Continuous production of 1,4-pentanediol from ethyl levulinate and industrialized furfuryl alcohol over Cu-based catalysts. *Sustain. Energy Fuels* **2022**, *6*, 2449–2461. [[CrossRef](#)]

Disclaimer/Publisher's Note: The statements, opinions and data contained in all publications are solely those of the individual author(s) and contributor(s) and not of MDPI and/or the editor(s). MDPI and/or the editor(s) disclaim responsibility for any injury to people or property resulting from any ideas, methods, instructions or products referred to in the content.